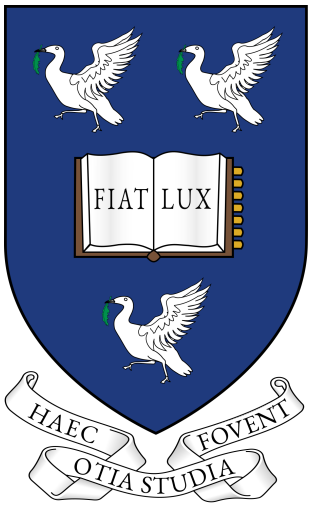

Double Binary as a Model of a Double Bar

A thesis submitted in partial fulfilment of the requirements
of the University of Liverpool for the degree of Bachelor of Science
by

George Scannell
(201458660)

Under the supervision of
Dr Witold Maciejewski

Department of Physics
The University of Liverpool
May 2022

Contents

I hereby declare that this thesis is my own work and that it has not been submitted elsewhere for any award. Where other sources of information have been used, they are acknowledged.

13/05/2022

Abstract

This project aimed to numerically simulate the dynamic motion of a double bar system within a double barred galaxy, as a function of the parameters which consist of the masses of the constituents and lengths of the bars. The specific results are the radius and angular velocity oscillations of the bars as they orbit around the galaxy. With regards to the results, it was found that as the central mass of the system was decreased the oscillations of the bars both increased. This increase eventually flattened out as the central mass became insignificant in value. As the mass of the inner bar was decreased, the inner bar oscillations increased slowly, whereas those for the outer bar decreased rapidly in comparison. As the initial radius of the outer bar was decreased, the oscillation of the two bars rapidly rose (quasi-exponential). The nature of this growth is not yet fully understood. These findings were thereafter applied to real barred galaxies by comparing torque values referenced in [1]. Overall, the project was a success. The main possible improvement for the future is with regards to the algorithm which determined the optimal initial velocities of the bars. A better algorithm will permit the exploration of more unstable parameters. To help validate the results, a barred galaxy survey could be carried out which searches for bars which follow the findings of this project.

1 Introduction

1.1 Background

The Observable Universe is estimated to harbour an approximate 200 Billion Galaxies [2]. These take form as a multitude of different morphologies. In general terms, there are three main types: Elliptical, Spiral and Irregular. All other observed forms can be considered as variations of these three. One such variant of the spiral galaxy is the **Barred** spiral galaxy (pictured below), which is the subject of research for this project.

Figure 1: Barred Spiral galaxy NGC 1300 - Hubble Space Telescope; https://hubblesite.org/contents/media/images/2005/01/1636-Image.html

Barred spirals earn their name because of the centrally located Bar structure they possess. This 'Bar' impacts the motions of stars and gas within the galaxy, for example by pulling gas onto elongated orbits towards the galactic centre, as can be seen in the above figure as the streams of material travelling inwards from the bases of the spiral arms. Barred spirals are a common form of

galaxy, they are thought to be part of the natural evolution of spiral galaxies [3]. Up to two thirds of all spirals are estimated to house a Bar [4]. Our own galaxy, the Milky Way, has one.
Of these barred galaxies, an estimated 30% contain a smaller secondary Bar which lies within the (original) primary [5]. These are known as double-barred galaxies. The below figure provides an example of one such galaxy.

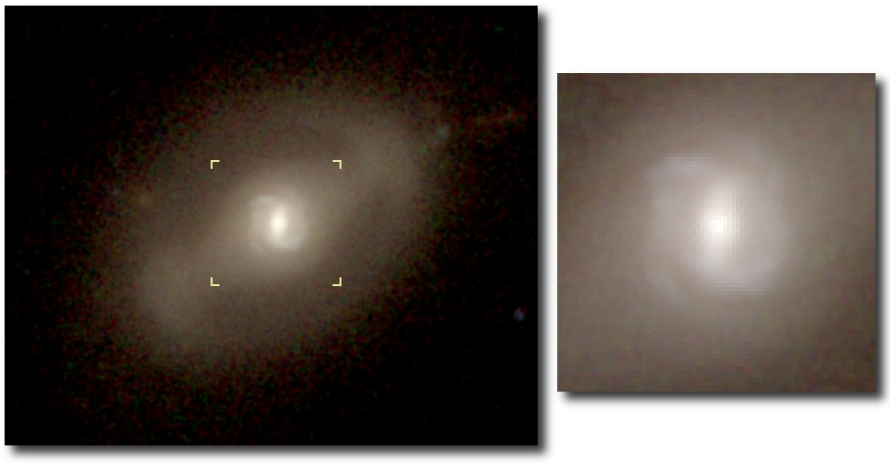

Figure 2: Double Barred galaxy GOODS J033230.93-273923.7 - Thorsten Lisker et al. https://www.mssl.ucl.ac.uk/~ipf/Media/Bar.html

1.2 How Bars are Formed

The Toomre Stability Criterion defines the Toomre Parameter as $Q = \frac{\sigma_R \kappa}{3.36 G \Sigma}$, where σ_R = Radial Velocity Dispersion, κ = Epicyclic Frequency, G = Gravitational Constant and
Σ = Surface Density. This defines the stability of a rotating stellar disk, which can be seen pictured below (first figure on left). Through simulations of rotating disks, it is determined that the threshold for collapse into a Bar system is when $Q = 1.2$. If realistic values for the early stages of a spiral galaxy are input into the Toomre Equation, the result is that many early spiral galaxies have a Q value which is below the threshold of 1.2. Therefore, they collapse into a (more stable) spiral bar formation. This is presented sequentially below, where the axially symmetric disk of rotating stars (left) evolves into a bar with spiral arms protruding from its ends.

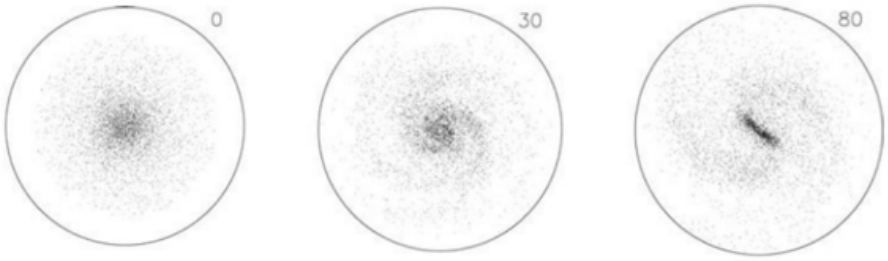

Figure 3: Bar Formation Example

Once a primary Bar has formed, it becomes a possibility that a secondary one can form also. The high torque at the ends of the Bars (as seen in Figure 3) pulls gas off of their circular orbits,

towards the centre of the galaxy (assuming the galaxy contains both stars **and** gas). Since Gas is much more collisional than stars are, it will collide amongst itself whilst travelling towards the centre. The collisions cause the gas to lose kinetic energy and therefore angular momentum, which will in turn reduce the orbital radii of the gas, confining it to relatively circular orbits close to the centre of the galaxy. As a consequence, another disk of rotating gas now resides around the core of the galaxy. Over time, this naturally turns into a disk of stars. The previous logic will therefore apply, where if the Toomre Parameter $Q < 1.2$, a Bar is formed. The result (if formed) is a large 'Primary' Bar and a smaller 'Secondary' Bar which lies within, at a much smaller size. These two structures rotate independently relative to each other.

1.3 Aims of this Project

This project sets out to study the dynamic effects of Primary and Secondary Bars within a double-barred spiral galaxy. These effects will present themselves as oscillations of the lengths and accelerations of the Bars as they rotate around each other. The desired results are plots which present the Radii and Angular Velocity changes of the Bars as a function of time, as they rotate about the centre of their host galaxy. The two Bars will be simulated with use of a numerical model. There are two avenues of study:

- Exploring the parameter space by self defining values (masses and lengths of the Bars) and varying them to see how the system acts as these are changed (radii and angular velocities)
- Use real, researched parameters of Barred Galaxies to see how the Bars in a spiral galaxy act in reality (based on the model). The results can be used to solidify/improve understanding of Barred spiral galaxies through existing data, and aims to help explain certain effects which the Bars may cause.

2 Method

2.1 The Model

Performing the Numerical Model in an N-Body fashion (model individual 'particles' which represent groups of stars) was deemed inappropriate for this project for two reasons:

- N-Body simulations of the past encountered difficulty in controlling the formation of a secondary Bar - this will make it challenging to explore the parameter space in any way (main aim of the project).
- Simulating a substantial quantity of 'particles' (groups of many stars) will be impossible to model with good resolution given the equipment available (personal computer), since past N-Body simulations required the use of supercomputers.

Due to these constraints, several assumptions/simplifications of the system will need to be made:

- The high torque at each end of the Bars is responsible for a great portion of the effects that the Bars cause on their surroundings. With this in mind, it is not unreasonable to say that each Bar can be (roughly) approximated as a binary, with half of its mass at one end and half at the other (a pair of binary stars)

- Since Bars are observed to be straight in nature, a condition of the system can be set whereby one end of the Bar oppositely mirrors the other ends' movement i.e. the Bar (binary) is symmetrical about the origin
- A heavy, unmoving mass can be defined as the origin (0,0). This can be interpreted as the combined mass of the galactic bulge (dense population of stars) and the Supermassive Black Hole which inhabit the core of the galaxy.

The figure below portrays the simplifications of this Double Bar system, whereby the heavy central mass (M) is orbited by the two binary pairs (m_1,m_2 and m_3,m_4) which rotate independently. It is noted how the Bars are mirrored about the origin ($x_1 = -x_3$, $y_1 = -y_3$, $x_2 = -x_4$, $y_2 = -y_4$) and that $m_1 = m_2$ and $m_3 = m_4$. The Black Lines aim to portray the whole Bar (will not be modelled) and are simply there as a reference for where the Bars would be in reality.

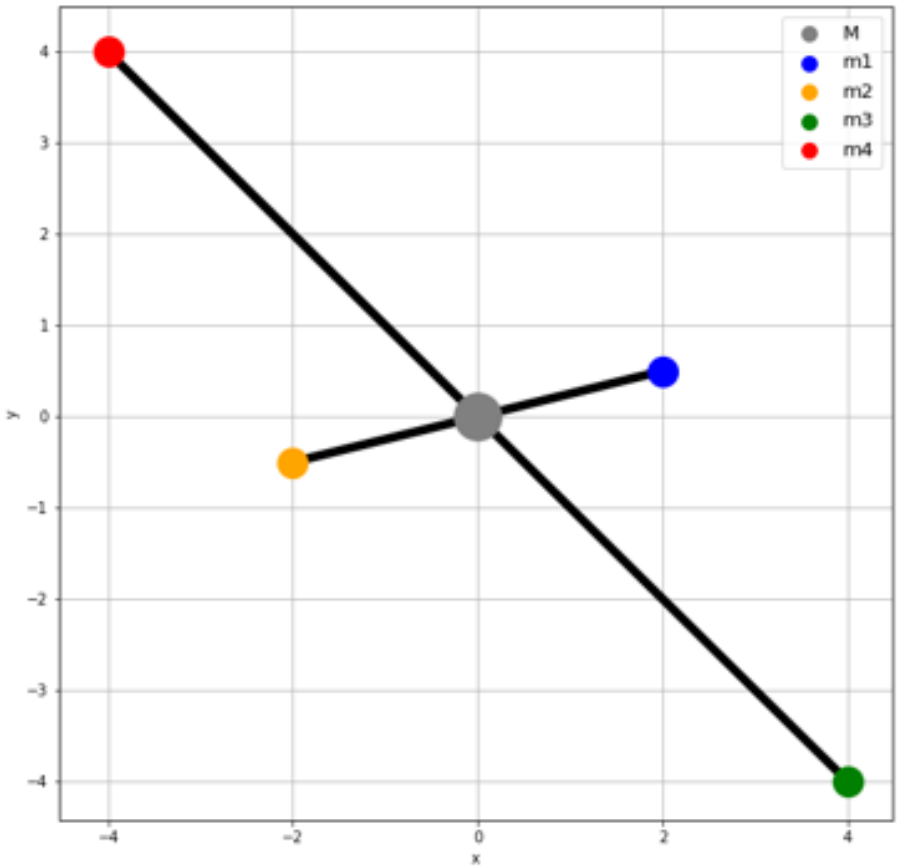

Figure 4: Double Bar System Simplification

2.1.1 Equations of Motion

There are four bodies in motion in this model. These are paired within their bars so that they **oppositely** mimic the movement of one another (if one moves to $x = 5$, the other moves to $x = -5$). This means that we need to create four sets of gravitational equations: Two describing the x and y movement of a star on the inner bar, and similarly two for the x and y of a star on the outer bar (Cartesian coordinates are used opposed to polar for calculation simplicity in working out the forces

between the Bars). The below illustration highlights the process of working out the components of forces on the masses - with use of trigonometry.

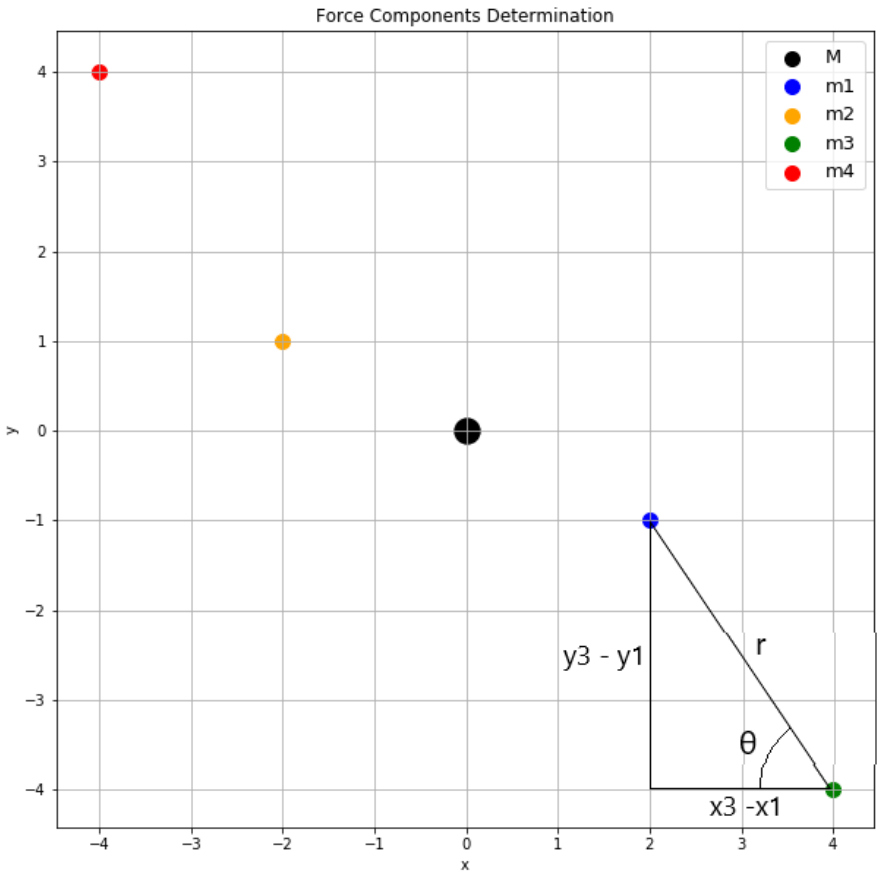

Figure 5: Graph showing how the force components are determined

The mock-up of the double bar orbital system shown above focuses on the force between masses m_1 and m_3 (blue and green). The x component of a force between two objects is the total force multiplied by the cosine of the angle between the objects. Contrastingly, the y component is the force times the sin of the angle between them. Below, the expressions for the x and y components of the force **acting on m1** (blue) are shown, substituting for r and the difference in x and y, as per the triangle, instead of using the angle (Cartesian environment). x and y denote the coordinate of the object in question, whereas x' and y' denote the object which is acting on said point of question:

$$F_x = F\cos\theta = F\frac{Adjacent}{Hypotenuse} = F\frac{x'-x}{r} = \frac{GMm}{r^3}(x'-x) = \frac{Gm_1m_3(x_3-x_1)}{\left(\sqrt{(x_3-x_1)^2+(y_3-y_1)^2}\right)^3} \tag{1}$$

$$F_y = F\sin\theta = F\frac{Opposite}{Hypotenuse} = F\frac{y'-y}{r} = \frac{GMm}{r^3}(y'-y) = \frac{Gm_1m_3(y_3-y_1)}{\left(\sqrt{(x_3-x_1)^2+(y_3-y_1)^2}\right)^3} \tag{2}$$

This leads to the equations for the accelerations of the stars (below), which will be utilised and solved in the program. Of course, to find the total acceleration for a star, the equations will have to be summated with respect to all of the stars in the system:

$$a_x = \frac{d^2x}{dt^2} = \frac{F_x}{m} = \sum_i \frac{GM_i}{{r_i}^3}\left({x_i}' - x\right) \tag{3}$$

$$a_y = \frac{d^2y}{dt^2} = \frac{F_y}{m} = \sum \frac{GM_i}{{r_i}^3}\left({y_i}' - y\right) \tag{4}$$

The total equations of motion for stars 1 and 3 are shown below. It is noted that instead of using for example x_4 or m_4, the equal counterparts $-x_3$ and $m3$ are implemented, in order to simplify the number of variables.

$$\begin{aligned}\frac{d^2x_1}{dt^2} &= \frac{GM\left(0-x_1\right)}{\left(\sqrt{x_1^2+y_1^2}\right)^3} + \frac{Gm_2\left(x_2-x_1\right)}{\left(\sqrt{\left(x_2-x_1\right)^2+\left(y_2-y_1\right)^2}\right)^3} + \frac{Gm_3\left(x_3-x_1\right)}{\left(\sqrt{\left(x_3-x_1\right)^2+\left(y_3-y_1\right)^2}\right)^3} + \frac{Gm_4\left(x_4-x_1\right)}{\left(\sqrt{\left(x_4-x_1\right)^2+\left(y_4-y_1\right)^2}\right)^3} \\ &= \frac{GM\left(-x_1\right)}{\left(\sqrt{x_1^2+y_1^2}\right)^3} + \frac{Gm_1\left(-2x_1\right)}{\left(2\sqrt{x_1^2+y_1^2}\right)^3} + \frac{Gm_3\left(x_3-x_1\right)}{\left(\sqrt{\left(x_3-x_1\right)^2+\left(y_3-y_1\right)^2}\right)^3} + \frac{Gm_3\left(-x_3-x_1\right)}{\left(\sqrt{\left(-x_3-x_1\right)^2+\left(-y_3-y_1\right)^2}\right)^3}\end{aligned} \tag{5}$$

$$\begin{aligned}\frac{d^2y_1}{dt^2} &= \frac{GM\left(0-y_1\right)}{\left(\sqrt{x_1^2+y_1^2}\right)^3} + \frac{Gm_2\left(y_2-y_1\right)}{\left(\sqrt{\left(x_2-x_1\right)^2+\left(y_2-y_1\right)^2}\right)^3} + \frac{Gm_3\left(y_3-y_1\right)}{\left(\sqrt{\left(x_3-x_1\right)^2+\left(y_3-y_1\right)^2}\right)^3} + \frac{Gm_4\left(y_4-y_1\right)}{\left(\sqrt{\left(x_4-x_1\right)^2+\left(y_4-y_1\right)^2}\right)^3} \\ &= \frac{GM\left(-y_1\right)}{\left(\sqrt{x_1^2+y_1^2}\right)^3} + \frac{Gm_1\left(-2y_1\right)}{\left(2\sqrt{x_1^2+y_1^2}\right)^3} + \frac{Gm_3\left(y_3-y_1\right)}{\left(\sqrt{\left(x_3-x_1\right)^2+\left(y_3-y_1\right)^2}\right)^3} + \frac{Gm_3\left(-y_3-y_1\right)}{\left(\sqrt{\left(-x_3-x_1\right)^2+\left(-y_3-y_1\right)^2}\right)^3}\end{aligned} \tag{6}$$

$$\begin{aligned}\frac{d^2x_3}{dt^2} &= \frac{GM\left(0-x_3\right)}{\left(\sqrt{x_3^2+y_3^2}\right)^3} + \frac{Gm_4\left(x_4-x_3\right)}{\left(\sqrt{\left(x_4-x_3\right)^2+\left(y_4-y_3\right)^2}\right)^3} + \frac{Gm_1\left(x_1-x_3\right)}{\left(\sqrt{\left(x_1-x_3\right)^2+\left(y_1-y_3\right)^2}\right)^3} + \frac{Gm_2\left(x_2-x_3\right)}{\left(\sqrt{\left(x_2-x_3\right)^2+\left(y_2-y_3\right)^2}\right)^3} \\ &= \frac{GM\left(-x_3\right)}{\left(\sqrt{x_3^2+y_3^2}\right)^3} + \frac{Gm_3\left(-2x_3\right)}{\left(2\sqrt{x_3^2+y_3^2}\right)^3} + \frac{Gm_1\left(x_1-x_3\right)}{\left(\sqrt{\left(x_1-x_3\right)^2+\left(y_1-y_3\right)^2}\right)^3} + \frac{Gm_1\left(-x_1-x_3\right)}{\left(\sqrt{\left(-x_1-x_3\right)^2+\left(-y_1-y_3\right)^2}\right)^3}\end{aligned} \tag{7}$$

$$\begin{aligned}\frac{d^2y_3}{dt^2} &= \frac{GM\left(0-y_3\right)}{\left(\sqrt{x_3^2+y_3^2}\right)^3} + \frac{Gm_4\left(y_4-y_3\right)}{\left(\sqrt{\left(x_4-x_3\right)^2+\left(y_4-y_3\right)^2}\right)^3} + \frac{Gm_1\left(y_1-y_3\right)}{\left(\sqrt{\left(x_1-x_3\right)^2+\left(y_1-y_3\right)^2}\right)^3} + \frac{Gm_2\left(y_2-y_3\right)}{\left(\sqrt{\left(x_2-x_3\right)^2+\left(y_2-y_3\right)^2}\right)^3} \\ &= \frac{GM\left(-y_3\right)}{\left(\sqrt{x_3^2+y_3^2}\right)^3} + \frac{Gm_3\left(-2y_3\right)}{\left(2\sqrt{x_3^2+y_3^2}\right)^3} + \frac{Gm_1\left(y_1-y_3\right)}{\left(\sqrt{\left(x_1-x_3\right)^2+\left(y_1-y_3\right)^2}\right)^3} + \frac{Gm_1\left(-y_1-y_3\right)}{\left(\sqrt{\left(-x_1-x_3\right)^2+\left(-y_1-y_3\right)^2}\right)^3}\end{aligned} \tag{8}$$

2.1.2 Making an Equation Dimensionless

This section acts as a note on dimensionless equations, which will be of great benefit later on. Utilising dimensionless equations is extremely beneficial due to the fact that the input parameters need only be presented as proportionalities of each other. For example, the central mass can be input as $M = 10$ and the inner bar's mass as $M = 1$. This represents that they are different by a factor of 10. The solutions can then easily be scaled up an down (to give real world solutions) based upon the realistic size of the system which is being investigated, just by altering a given parameter which is based upon the constants in the equation. Shown below is the general equation for gravity which is utilised in the project, as well as the expressions for distance, mass and time, which will be used to make the equation dimensionless.

$$F = ma = m\frac{d^2r}{dt^2} = \frac{GMm}{r^2} \quad \Longrightarrow \quad \frac{d^2r}{dt^2} = \frac{GM}{r^2} \tag{9}$$

$$r = \hat{r} \cdot r_0 \qquad M = \hat{M} \cdot M_0 \qquad t = \hat{t} \cdot t_0 \tag{10}$$

The subscript 0 parameters are changed to be constants (units) which are associated with a reference value i.e. the size of the orbits, masses of the bars or period of the orbits. These are multiplied by the proportionate set of (hat) variables which will be defined in the code. This proportionality will carry through when acted on by the scaling parameter. The equation for gravitational acceleration (Equation 9) then takes the form as follows (inputting new variables):

$$\frac{d^2\left(\hat{r} \cdot r_0\right)}{d\left(\hat{t} \cdot t_0\right)^2} = \frac{G\left(\hat{M} \cdot M_0\right)}{\left(\hat{r} \cdot r_0\right)^2} \quad \Longrightarrow \quad \frac{r_0}{t_0^2}\frac{d^2\hat{r}}{d\hat{t}^2} = \frac{M_0}{r_0^2}\frac{G\hat{M}}{\hat{r}^2} \tag{11}$$

We are now left with an equation which resembles the original equation for gravity, albeit with a number of constants (r_0, t_0 and M_0). If this equation was wanted in a dimnesionless form, a constraint must be placed which makes all of the constants equal each other, so that they cancel out. For example, when these coefficient are equated, G takes the form as:

$$G = \frac{r_0^3}{M_0 \cdot t_0^2} \tag{12}$$

Notice how if this G value is input back into the equation, all of the constants cancel out. With this equation in mind, if (for example) a more realistic time unit was wanted, the equation could be rearranged for t_0. Then, real scale values such as r_0 (kpc) and M_0 (M_{Sun}) can be input. This gives a time unit which goes as:

$$t_0 = \sqrt{\frac{\text{kpc}^2}{GM_{\text{Sun}}}} \tag{13}$$

So, there are two independent dimensional units (r and M in the previous example) and one free dimensional parameter (t in the previous example). For completeness, the **dimensionless** equations for the acceleration of gravity in the x and y directions takes the form as follows (no G value):

$$\frac{d^2\hat{x}}{d\hat{t}^2} = \sum_i \frac{\hat{M}_i}{\hat{r}_i{}^3}\left(\hat{x}_i{}' - \hat{x}\right) \tag{14}$$

$$\frac{d^2\hat{y}}{d\hat{t}^2} = \sum_i \frac{\hat{M}_i}{\hat{r}_i{}^3}\left(\hat{y_i}' - \hat{y}\right) \tag{15}$$

The above shows the acceleration felt from a combination of **all** of the mass constituents of the system. This means that the equations of motion at the bottom of 2.1.1 (in dimensionless form) will have no G value included. For example, Equation 5 becomes:

$$\begin{aligned}\frac{d^2x_1}{dt^2} &= \frac{M\left(0-x_1\right)}{\left(\sqrt{x_1^2+y_1^2}\right)^3} + \frac{m_2\left(x_2-x_1\right)}{\left(\sqrt{\left(x_2-x_1\right)^2+\left(y_2-y_1\right)^2}\right)^3} + \frac{m_3\left(x_3-x_1\right)}{\left(\sqrt{\left(x_3-x_1\right)^2+\left(y_3-y_1\right)^2}\right)^3} + \frac{m_4\left(x_4-x_1\right)}{\left(\sqrt{\left(x_4-x_1\right)^2+\left(y_4-y_1\right)^2}\right)^3} \\ &= \frac{M\left(-x_1\right)}{\left(\sqrt{x_1^2+y_1^2}\right)^3} + \frac{m_1\left(-2x_1\right)}{\left(2\sqrt{x_1^2+y_1^2}\right)^3} + \frac{m_3\left(x_3-x_1\right)}{\left(\sqrt{\left(x_3-x_1\right)^2+\left(y_3-y_1\right)^2}\right)^3} + \frac{m_3\left(-x_3-x_1\right)}{\left(\sqrt{\left(-x_3-x_1\right)^2+\left(-y_3-y_1\right)^2}\right)^3}\end{aligned} \tag{16}$$

2.2 Parameters

2.2.1 Free Parameters

The Free Parameters of the System are the values which are manually input. The 'Forced' parameters (accelerations, velocities) proceed to be defined based upon these values. In this case, the free parameters are the individual masses of the system, as well as the initial positions of the Bars. Since the equations are dimensionless, these manually defined values are not valued in terms of any units (Solar masses, parsecs etc) - they are valued purely as proportions to each other.

As a reminder, the two main goals of this project are: Investigate the limits of stability for the model (explore parameter space); Simulate the dynamics of the Bars on a realistic basis. As a consequence of these goals, the Free Parameters will take on a wide range of values depending on what is being investigated. For the initial construction and testing of the model, it is imperative that the system is provided with parameters which take upon 'safe' values - ones which deliver a high level of stability without much external effort. These values can be relatively arbitrary. Once the system is proven stable in these conditions, the parameters space can then be investigated further to provide systems with greater instability. A clear way to do this is to construct the system so that the mass distribution decreases with radius i.e. The mass hierarchy goes as $M_{Central} > M_{Inner\,Bar} > M_{Outer\,Bar}$. Systems with these conditions naturally exhibit greater stability. The (arbitrary) values for masses and initial distances are presented below:

Table 1: Free Parameters (Mass and Initial Radius) of the Individual Objects of the System

Body	Mass (Dimensionless)	Initial Radius (Dimensionless)
Central Mass	20	0 (Fixed)
Inner Bar	4	1
Outer Bar	2	7

It was decided to initially make the Central Mass considerably more massive than the two Bars. This reduces the dynamics between the Bars, since the majority of their gravitational force will be

coming from the (unmoving) centre. This will naturally give greater stability since the Bars only have one main force affecting them, granting easier access to circular (stable) orbits. Also to be noted - in the calculations each individual half of the Bars will be considered. Therefore, the actual masses used for the ends of each Bar will be half of the quoted values in the table. For example, the mass of one end of the Inner Bar = 2.

To reiterate, the above quoted Free Parameters will be used as demonstration (example figures etc.) for the **method** section of this report (current section). In the **results** section, these will be changed to a variety of different values in order to investigate the parameter space of the model.

2.2.2 Initial Velocities

In order to study this system as intended, whereby the effects of one bar on another is observed, it is imperative that in the inertial frame (rest frame with respect to the central mass), the binaries follow the most constant orbits possible (constant radius and velocity). This is because if a binary which follows a non-circular orbit is viewed within the reference frame of the other, it will be difficult to distinguish if any variation in radius/angular velocity is being caused by a general Keplerian ellipticity (free oscillation), or by the more nuanced gravitational effect of one bar on the other (forced oscillation).

A reasonable place to start is by trying to set the initial velocities so that (initially) the binaries are moving as if they are on circular orbits (they wont be because of how they interact). This can be achieved by (for each binary) equating the equations of motion for gravity with those of circular motion. If the force of gravity is equal to that of centripetal force, the mass must by definition be moving with constant velocity (speed) - a value which can be extracted from the equations. Since star 2 mimics star 1 (as star 4 also does for star 3), it is only necessary to work out the velocities for stars 1 and 3. The velocities of stars 2 and 4 will simply be the opposite of their counterparts. The stars are initialised so that they all lie on the x axis, for simplicity of calculation (the variable r only needs to be in terms of x). A representation of this is shown in a figure below:

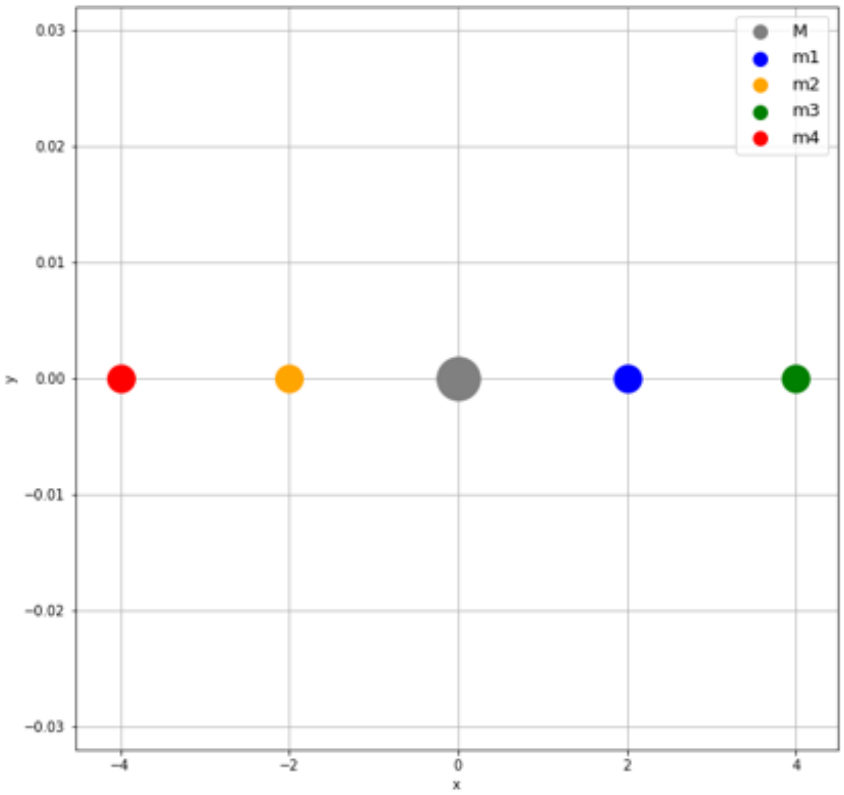

Figure 6: System Arrangement to find the Initial Velocities

The below block of equations describe the methodology behind working out the optimal velocities for the bars. Note that d is the distance to the point of rotation (origin) whereas r is the distance to each particular star.

$$F_{Gravity} = \sum \frac{GMm}{r^2} = F_{Centripetal} = \frac{mv^2}{d} \tag{17}$$

$$\text{Cancelling } m\text{:} \quad \sum \frac{GM}{r^2} = \frac{v^2}{d} \implies v = \sqrt{d \sum \frac{GM}{r^2}} \tag{18}$$

$$\begin{aligned} \text{Star 1 Velocity} &= \sqrt{x_1 \left(\frac{GM}{(x_1)^2} + \frac{Gm_2}{(x_2 - x_1)^2} - \frac{Gm_3}{(x_3 - x_1)^2} + \frac{Gm_4}{(x_4 - x_1)^2} \right)} \\ &= \sqrt{x_1 \left(\frac{GM}{(x_1)^2} + \frac{Gm_1}{(2x_1)^2} - \frac{Gm_3}{(x_3 - x_1)^2} + \frac{Gm_3}{(x_3 + x_1)^2} \right)} \end{aligned} \tag{19}$$

$$\begin{aligned} \text{Star 3 Velocity} &= \sqrt{x_3 \left(\frac{GM}{(x_3)^2} + \frac{Gm_4}{(x_4 - x_3)^2} + \frac{Gm_1}{(x_3 - x_1)^2} + \frac{Gm_2}{(x_2 - x_3)^2} \right)} \\ &= \sqrt{x_3 \left(\frac{GM}{(x_3)^2} + \frac{Gm_3}{(2x_3)^2} + \frac{Gm_1}{(x_3 - x_1)^2} + \frac{Gm_1}{(-x_1 - x_3)^2} \right)} \end{aligned} \tag{20}$$

Noted is the negative term within the calculation for star 1, and the contrastingly positive term in star 3's calculation. This is the case due to the layout of the system - For star 3's calculation, all of the other stars command their force in the same direction (left) and so they all have the same sign. For star 1's calculation, the relative location of star 3 is to the right (opposite direction to other stars), and so the sign will be the opposite compared to the others, in order to represent how it counteracts the forces of the other stars.

Due to the $t = 0$ nature of this calculation, the velocities are not given a complete direction, only the condition that they act tangential to their orbit. Since they are at $x = 0$, and the orbits are assumed circular, this means that their directions can be individually defined as either up (positive y) or down (negative y). It was decided for both velocities to be arbitrarily defined so that they point upwards (positive y) in order for the Bars to orbit anti-clockwise and follow the standard convention of angles increasing with anti-clockwise motion. Also, it was required for them both to orbit in the same direction since this is what the current scientific intuition predicts, based on the fact that the two bars form from the same initial (rotating) disk, therefore meaning they will both rotate in the same direction as their progenitor disk.

2.3 The Code

To start, the numerical simulation will be performed in Python due to the University's proclivity towards this specific language; having been the language which has been taught for the past three years. Modelling this system requires the function 'odeint', a numerical integrator which resides within the 'scipy' package of python (https://docs.scipy.org/doc/scipy/reference/generated/scipy.integrate.odeint.html). The function acts to integrate ordinary differential equations, as per its name. It takes as basic parameters: The function which describes the system (equations of motion), the initial conditions (velocities and positions), and the time period over which the model will be run. A slight complication is that it only has the ability to solve **First Order** differential equations, whereas the equations to be solved in this project are **Second Order** (since accelerations are being dealt with). This problem is resolved by writing the second order acceleration equation as two sets of coupled first order ODEs, effectively splitting the equation. Shown below with the example of acceleration a in one dimension x:

$$a = \frac{d^2x(t)}{dt^2} \quad \Longrightarrow \quad \begin{aligned} a &= \frac{dv(t)}{dt} \\ v(t) &= \frac{dx(t)}{dt} \end{aligned} \tag{21}$$

So, the functions input into 'odeint' will be $\frac{dv(t)}{dt}$ and $\frac{dx(t)}{dt}$. These will be integrated (over the time period) by the code, and will therefore output $v(t)$ and $x(t)$. Regarding the method of integration, 'odeint' defaults to the 'LSODA' algorithm, a Fortran based method which is unique in that it automatically switches between methods which can solve stiff (**unstable** for large time-steps) or non-stiff (**stable** for large time-steps) differential equations (program may become 'stiff' when unstable parameters are investigated). It also uses a linear multi-step (changes step size based on stability of coming steps), which is very useful since this system will be relatively unstable/chaotic due to the multitude of objects which all interact with each other - some sections of the simulation may need very small steps, others not as much (reduces computational time when stable periods are encountered).

Drawing on the (now obtained) items which are required to run the system: The derived equations of motion (Equation 5, Equation 6, Equation 7 and Equation 8 - without the G values since dimensionless) and initial velocities (Equation 19 and Equation 20), the simulation can now be run in an exploratory manner. As a further article into how the program finds the solutions to the system, referenced is Equation 21 shown above. Since the gravitational equations need to be split, input as the function parameter in 'odeint' will need to be the accelerations a for each bar (m1 and m3) for each direction (x and y). Also needed as input are the velocities for each bar, in each direction. All in all, an array of length 8 is input into 'odeint' as the function. It has a form as follows (v = velocity, a = acceleration):

$$\text{Odeint Function} = [\, v_{m1,x} \,|\, v_{m1,y} \,|\, a_{m1,x} \,|\, a_{m1,y} \,|\, v_{m3,x} \,|\, v_{m3,y} \,|\, a_{m3,x} \,|\, a_{m3,y} \,] \tag{22}$$

An array of equal length will also have to be submitted as the initial conditions parameter. Since the initial conditions take the form of the integrated function, needed as input are the initial positions and velocities for both bars (stars m1 and m3). Note how these are located within the array at the same index as their corresponding integrand is (Equation 22). The array takes the following form:

$$\text{Initial Conditions} = [\, x_{m1} \,|\, y_{m1} \,|\, v_{m1,x} \,|\, v_{m1,y} \,|\, x_{m3} \,|\, y_{m3} \,|\, v_{m3,x} \,|\, v_{m3,y} \,] \tag{23}$$

As previously stated in Table 1, the masses and initial positions contained there will be used as example for this current **method** section of the report, but will be varied in the **results** section to explore the parameter space. Those values can be combined in the initial velocity equations (2.2.2) to additionally find the initial velocities in the above array.

The time parameter of 'odeint' is relatively arbitrary, since it has minimal effect on the system. As long as it is not too short that any sought after effects are negligible/too small to be seen, or too long that the data is unreadable/the system becomes too unstable, its value is fine to choose non-methodically. An arbitrary requirement of 'at least a couple' orbits being completed (for the outer bar) was used. This baseline value used allowed data for at least an entire period of both bars to be recorded (Inner bar completes a period quicker due to its lower orbit). In this current case, the time was defined as $t = 50$ Units. Shown below is a plot of the system, produced with the function 'odeint', which is used in conjunction with the previously mentioned initial values and the equations of motion. As previously mentioned, the 'mirrored' halves of the two bars are made to act oppositely in comparison to their counterpart i.e starting position is on the other side, velocity is in the other direction. The orbits of each end of the Bars are plot individually (Inner Bar = m_1,m_2; Outer Bar = m_3,m_4):

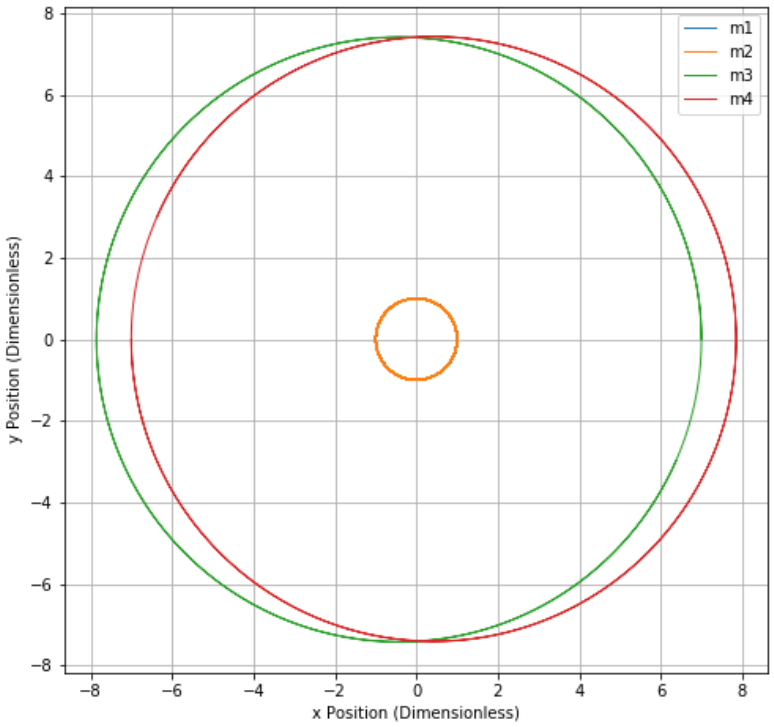

Figure 7: Preliminary plot of the orbits of the Bars (50 time units)

An animation of this plot can also be found here: https://theuniversityofliverpool.sharepoint.com/:v:/s/PHYS379-202122-II-0365-Team-Scannell/EfYo5_GwO0BBt3RjHbSpLHsB6ICvwxF1_YSh6hQ_2senng?e=A9zFsp. The coloured dots represent the ends of each bar.

As can be seen, the program performs the numerical model within expectations. The orbits of each bar are clearly visible, with the outer bar visually operating on a more elliptical orbit than the inner bar. In fact, the orbit of the inner bar is sufficiently circular that only the plot for one side of the binary (m_2) can be seen.

To more precisely analyse the ellipticity of the bars, a plot of the radius as a function of rotation angle about the origin (for both bars) can be created. The angle about the origin can be determined through trigonometry, with the arctangent of the x and y coordinates, as follows:

$$tan\,\theta = \frac{Opposite}{Adjacent} = \frac{y}{x} \quad \Longrightarrow \quad \theta = arctan\left(\frac{y}{x}\right) \tag{24}$$

The standard arctangent function cannot completely decipher the rotational position of a point on an axes. This is because (for example) the fraction $\frac{y}{x}$ for two coordinates (10,5) and (-10,-5) both equates to the same value (2). Of course, this means that the same angle will be output for the two. It is clear that it cannot understand the sign of each individual coordinate, only the overall sign of the resultant fraction $\frac{y}{x}$. With this logic, it will only be able to output angles for

two quadrants of a circle - from $-\frac{\pi}{2}$ to $\frac{\pi}{2}$. This result is undesired because the full rotation (2π) of the Bar is being studied. To resolve this, a modified version of arctan, named 'arctan2' is used within python https://numpy.org/doc/stable/reference/generated/numpy.arctan2.html. It intelligently looks at the sign of the coordinates, and is able to output a full range of angles from $-\pi$ to π (full range of 2π).

For completeness, the radius value at each point is derived through the x and y coordinates, with use of the Pythagorean Theorem. The calculation is simplified since the origin is located at (0,0), meaning that no coordinate differences need to be found:

$$a^2 + b^2 = c^2 \quad \Longrightarrow \quad r^2 = x^2 + y^2 \Longrightarrow \quad r = \sqrt{x^2 + y^2} \tag{25}$$

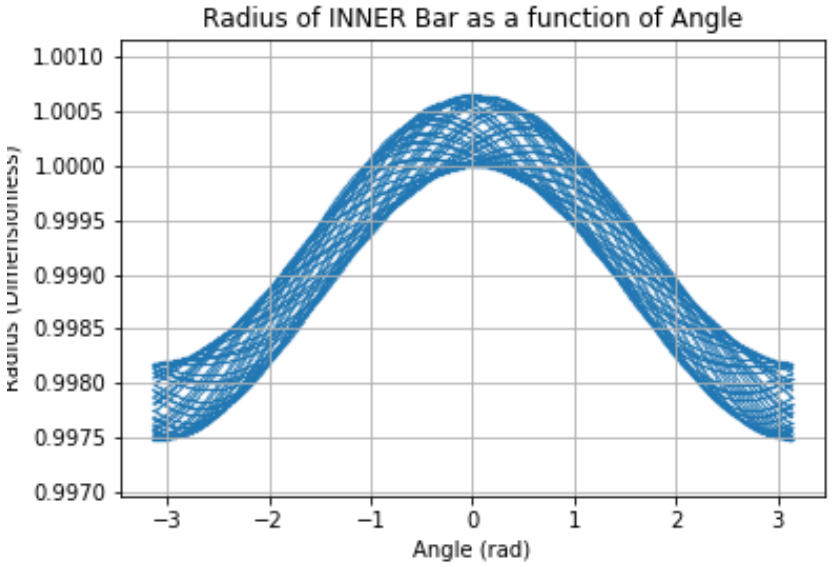

Figure 8: Radius of Inner Bar as a function of rotational angle (50 time units)

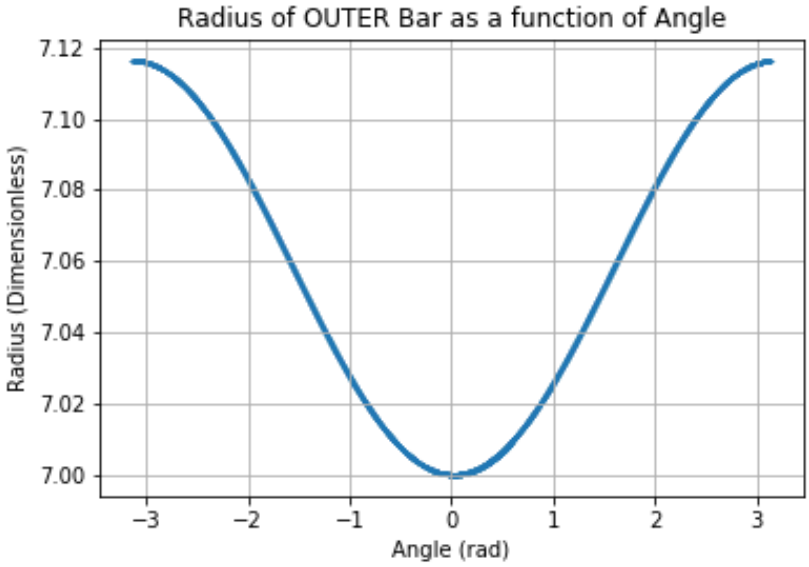

Figure 9: Radius of Outer Bar as a function of rotational angle (50 time units)

Spanning from angle $-\pi$ to π, these graphs tell a much better story of how the radii of the Bars behave over time. It is noted that the Inner Bar has a much less defined plot than the outer bar. This 'thickening' of the radius plot is a result of the interaction with the outer bar (forced oscillation). At this scale, the forced oscillation effect is not seen clearly on the outer bar. The overall non-circularity of the orbits of both bars are dominated by free oscillations (outer bar more so). Clearly, the routine whereby the gravitational and centripetal Forces were equaled was not enough to minimise the free oscillation of the Bars. This is shown by the overall trend of both bars to be non-constant. This has occurred because the optimised velocity calculations were performed at $t = 0$, where the masses are all lines up on the x axis (forces all in same plane). As soon as the system starts running the ideal (circular) velocities change since now there are constantly varying x and y force components which are a result of the angular differences between the Bars (Inner Bar rotates quicker since it is closer to the origin). Therefore, the orbits fall out of circularity. All in all, this is a good start for a model of the system. Particular parameters (initial velocities) now need to be fine-tuned so that the Bars keep a more constant radius over the simulation period.

2.3.1 Energy Conservation

Before moving on, it is important to take a step back and quantitatively check if the system is working correctly. A good way of confirming this is by checking if the law of energy conservation is held. If the total kinetic energy added to the total potential energy of the system stays the same with time, this means that the law is followed, and the program can reliably be used to model a real life system. There will naturally be some oscillation/deviation due to the approximate nature of this simulation (numerical), but it should still stay within a certain (small) range over a period of time. Below, the equation for energy conservation is shown.

$$\sum E_k + \sum E_p = \text{Constant} \tag{26}$$

Where $E_k = \frac{1}{2}mv^2$ and $E_p = -\frac{GMm}{r}$

$$\begin{aligned}\sum E_k &= \frac{1}{2}m_1\left(v_{x,1}^2+v_{y,1}^2\right)+\frac{1}{2}m_2\left(v_{x,2}^2+v_{y,2}^2\right)+\frac{1}{2}m_3\left(v_{x,3}^2+v_{y,3}^2\right)+\frac{1}{2}m_4\left(v_{x,4}^2+v_{y,4}^2\right)\\ &= m_1\left(v_{x,1}^2+v_{y,1}^2\right)+m_3\left(v_{x,3}^2+v_{y,3}^2\right)\end{aligned} \tag{27}$$

It is important to note that within a gravitational system of multiple objects, the potential energies are calculated in pairs, so as to not be repeated. For example, in a system of two stars a single potential energy is calculated, instead of two - corresponding to each respective stars' effect on the other. Essentially, we want it so that each star has been paired up to each other **only once**. To do this, I initially pair star 1 up with every other object. Moving on to star 2, I do the same except I **exclude** star 1 since that has already been calculated. For star 3, do the same but exclude both star 1 **and** 2 since they have both been calculated already, etc. The calculation is shown below. It is noted that I initially show the real label of the body ie. m_2, x_2 but change it to its equivalent m_1, $-x_1$ to signify the simplification and how it is actually performed in the code.

$$\begin{aligned}\sum E_{p,1} &= \frac{Gm_1M}{\sqrt{x_1^2+y_1^2}}+\frac{Gm_1m_2}{2\sqrt{x_1^2+y_1^2}}+\frac{Gm_1m_3}{\sqrt{(x_1-x_3)^2+(y_1-y_3)^2}}+\frac{Gm_1m_4}{\sqrt{(x_1-x_4)^2+(y_1-y_4)^2}}\\ &= \frac{Gm_1M}{\sqrt{x_1^2+y_1^2}}+\frac{Gm_1^2}{2\sqrt{x_1^2+y_1^2}}+\frac{Gm_1m_3}{\sqrt{(x_1-x_3)^2+(y_1-y_3)^2}}+\frac{Gm_1m_3}{\sqrt{(x_1+x_3)^2+(y_1+y_3)^2}}\end{aligned} \tag{28}$$

$$\begin{aligned}\sum E_{p,2} &= \frac{Gm_2M}{\sqrt{x_2^2+y_2^2}}+\frac{Gm_2m_3}{\sqrt{(x_2-x_3)^2+(y_2-y_3)^2}}+\frac{Gm_2m_4}{\sqrt{(x_2-x_4)^2+(y_2-y_4)^2}}\\ &= \frac{Gm_1M}{\sqrt{x_1^2+y_1^2}}+\frac{Gm_1m_3}{\sqrt{(-x_1-x_3)^2+(-y_1-y_3)^2}}+\frac{Gm_1m_3}{\sqrt{(-x_1+x_3)^2+(-y_1+y_3)^2}}\end{aligned} \tag{29}$$

$$\sum E_{p,3} = \frac{Gm_3M}{\sqrt{x_3^2+y_3^2}}+\frac{Gm_3m_4}{2\sqrt{x_3^2+y_3^2}} = \frac{Gm_3M}{\sqrt{x_3^2+y_3^2}}+\frac{Gm_3^2}{2\sqrt{x_3^2+y_3^2}} \tag{30}$$

$$\sum E_{p,4} = \frac{Gm_4M}{\sqrt{x_3^2+y_3^2}} = \frac{Gm_3M}{\sqrt{x_3^2+y_3^2}} \tag{31}$$

Therefore:

$$\sum E_p = \sum E_{p,1}+\sum E_{p,2}+\sum E_{p,3}+\sum E_{p,4} \tag{32}$$

The graph of total energy over time could then be made. A time of 500, rather than 50 (10x more) was used in order to see if the system could remain energetically stable for a more extended period of time, compared to that which will be used in the main analysis of the system (≈ 50). If it is well stable in the longer regime it gives great confidence when using using the smaller time periods, since they will naturally accumulate a smaller number of energy deviations. This essentially gives a safe upper limit on what time values can be used. Using the default 'odeint' accuracy parameters (leave space blank), the graph of total energy over 500 units of time was plot:

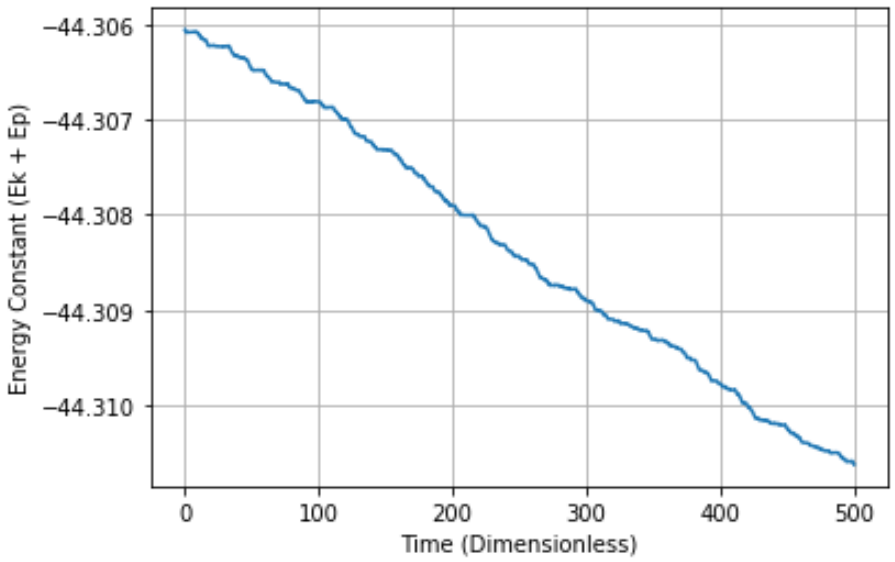

Figure 10: Total Energy of the System (500 time units)

The graph shows a clear downwards trend over time, where the total energy has decreased by 0.004 over the time period of 500. This is an accuracy level of $\approx 10^{-4}$ with regards to the average energy ≈ -44 (Calculated from the ratio between the two). This is small, but not small enough (the commonly accepted accuracy level is between 10^{-6} and 10^{-8}) The fact that the plot decreases almost monotonically highlights how the system's true constraints are not being tested. A more jagged/undefined curve would show that the program is working at its limits, since the total energy would be changing more unpredictably.

To increase the accuracy of the integration, certain parameters within 'odeint' can be altered - namely 'rtol', 'atol' and 'hmax'. The values 'rtol' and 'atol' both default to $1.49012e-08$ - they are involved in the error control of the function. Smaller values mean that the tolerances for the error will be smaller (increases accuracy). 'hmax' is defined as the maximum step that the function can take between points, its value is automatically decided (by odeint) with reference to the current system. Of course, reducing this will increase accuracy, as it will stop the program from cutting corners - making jumps that are too big with the aim to improve computational time. Below is a plot of the energy over the same time period, but with rtol $= 1.490\,12 \times 10^{-12}$, atol $= 1.490\,12 \times 10^{-12}$ and hmax $= 0.001$ (reduced values for accuracy):

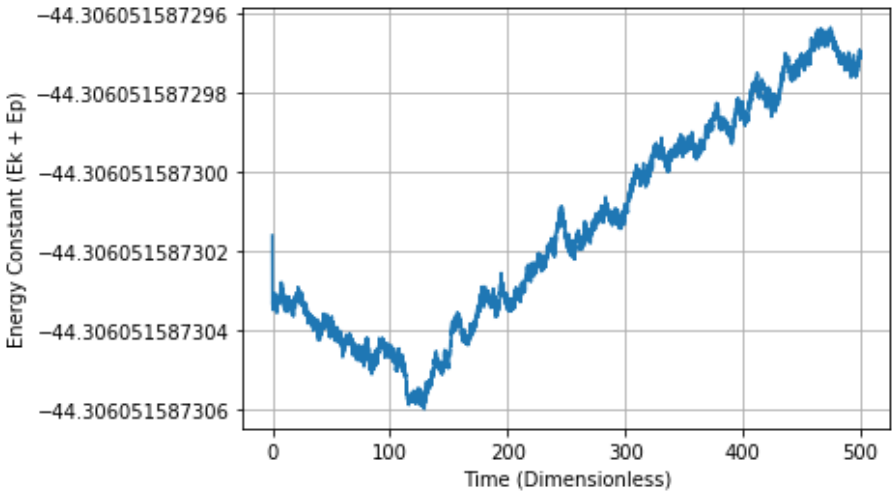

Figure 11: Total Energy of the System (500 time units) - Reduced 'rtol', 'atol' and 'hmax' values to increased accuracy

Clearly, the system is now conserving the total energy much better. The total changes by $\approx 10^{-11}$, with an overall accuracy $\approx 10^{-13}$, which is 9 orders of magnitude more accurate than the previous. The shape of the graph is much more erratic, showing that the system is now closer to its limits (also over a much smaller range). All in all, the model is confirmed to conserve energy well, especially when modifying the integration to be more accurate. In reality, these changes are not necessary, especially over the shorter time period which will be used in the actual analysis. This is because they lengthen the time of computation considerably (~ 1 second vs ~ 1 minute for the two graphs just shown respectively) in return for negligible differences in the results. This alteration is simply used as an indicator to show that the program **has the ability** to conserve the energy of the system to outstanding (unnecessary) precision.

2.4 Initial Velocity Correction

The initial velocities calculated through equalisation of the forces of gravity and circular motion are only estimates, due to the fact that when the program is ran the orbits are still not circular. Looking at the plots (Figure 8 and Figure 9), it is clear that the inner bar 'undershoots' its target - its initial velocity is too small, given that once having rotated 180 degrees or π (from the initial $\theta = 0$), its radius is smaller. Conversely, the outer bar 'overshoots' - its radius has increased at $180/\pi$ degrees of rotation. Clearly, both orbits are elliptical. To work towards resolving this, some vague trial and error was initially used (guessing values and checking the plots). It was apparent that if the velocities of the inner bar and outer bar were respectively made 1.0003 and 0.9727 times their initial suggested value (by Equation 19 and Equation 20), the orbits of the Bars (especially the Outer) were considerably more circular. Plots shown below:

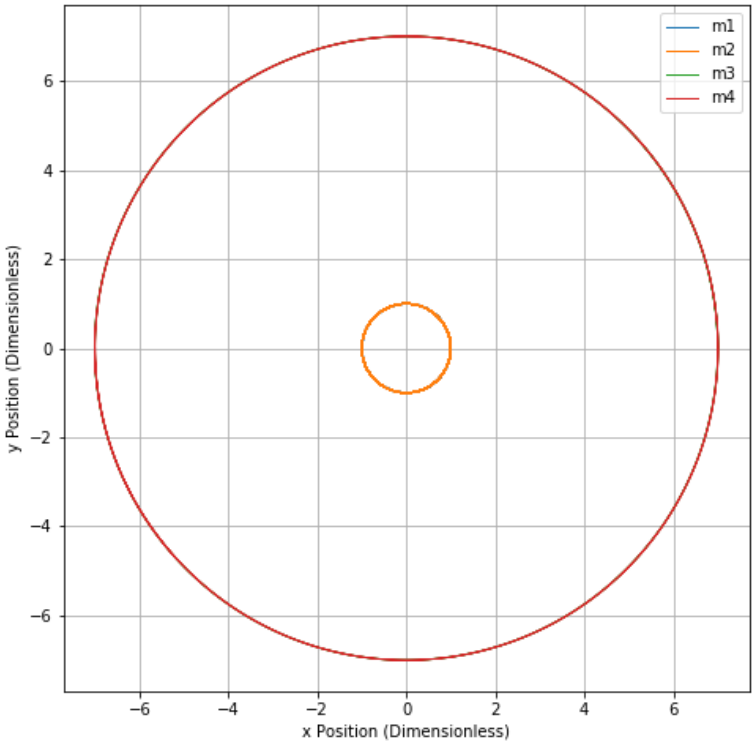

Figure 12: Orbits of the Bars with 'trial and error' modified velocities (50 time units)

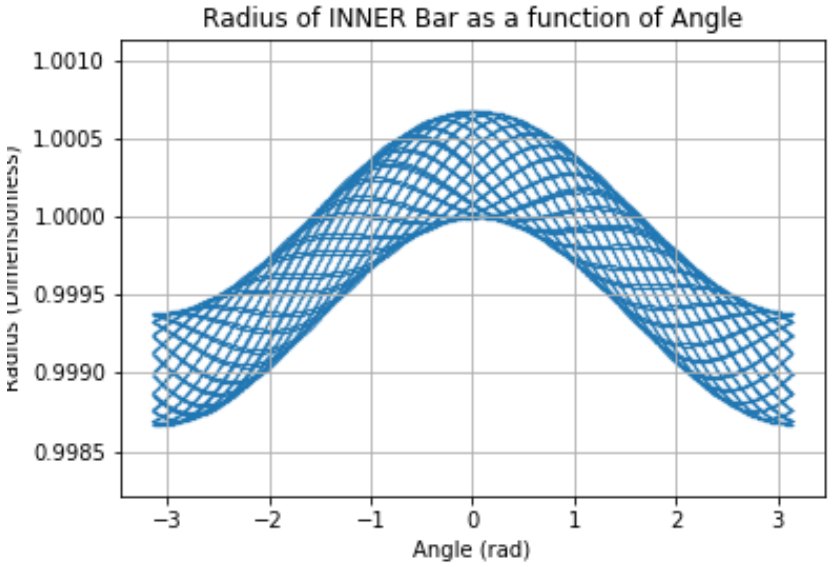

Figure 13: Radius of Inner Bar as a function of rotational angle, with trial and error modified velocities (50 time units)

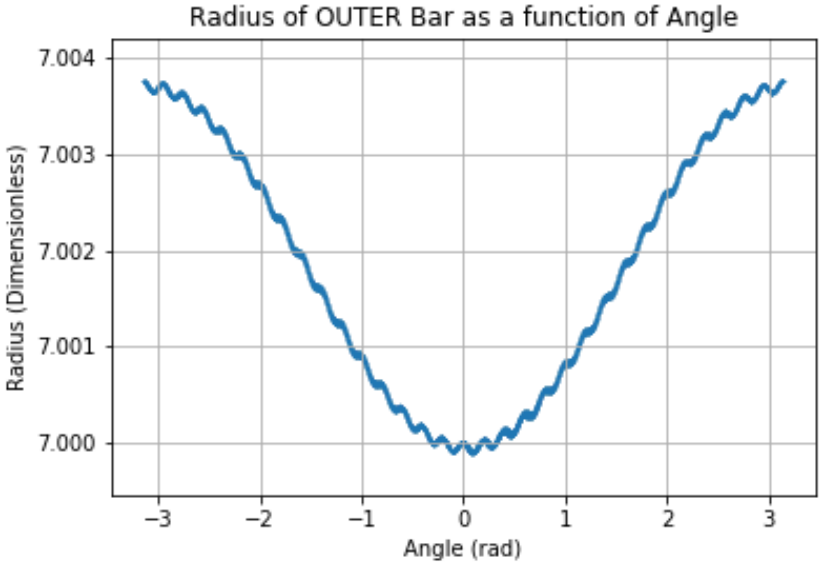

Figure 14: Radius of Outer Bar as a function of rotational angle, with trial and error modified velocities (50 time units)

With this reduced radius variation, the distinction between the effect of the Keplerian ellipticity (free oscillation) and the force of the other bar (forced oscillation) is becoming more visible. This is easily seen on the Outer Bar's figure - where a sinusoidal shape is beginning to take form on top of the general radius variation caused by the elliptical orbit. The intent thereafter is to completely remove the Keplerian ellipticity in order to exclusively study the effect caused by the other Bar.

Clearly, to make both bars keep a constant radius, the Inner Bar's velocity had to be increased, and the outer bar's velocity decreased. The question was, by how much? Trial and error would not be viable here, since it would take too long. Also, if the initial parameters were changed in any way the velocities would have to be painstakingly worked out again. An algorithm was required to solve this problem. It was first attempted to create two arrays of a vast range of velocities (100 each): one that included velocities above that of the inner bar, and one that included velocities below that of the outer bar. The goal was to attempt the integration with all possible combinations of these velocities, and pick the two velocities which gave the most constant radii for both bars. How 'constant' the radii were was determined by the standard deviation of the array containing all of the radius values over the set time period. This was not a good method due to the $100 \times 100 = 10000$ integrations needed to be performed, which took 10's of minutes (too long). In hindsight, the reason that it was ultimately unsuccessful in finding the velocity combination which minimised both radii deviations well, was due to the condition whereby the **sum** of the smallest radius deviations for both Bars was found. Since the Outer Bar deviated in radius by an order of magnitude greater than the Inner Bar, the program would naturally tend towards minimising the ellipticity of the Outer Bar alone, since the radius deviation of the Outer Bar would have a greater effect on the overall sum of the two Radii deviations of the Bars.

A more efficient computational method was needed for this task (preferably one that didn't complete in N^2 time). With some research, the most obvious choice was by using recursion. This is a method whereby the program starts with the initial velocity, changes it by a predetermined amount, runs the integration and then checks if the radius deviates by too much (standard deviation). 'Too much' is defined by an input value (arbitrary accuracy). If the radius deviation is below this value the program stops and returns the current velocity values. If the deviation is still above the given threshold, the program is run again. This approach seemed to work very well in some cases; it computed in only a few seconds. The downside is that the method was very sensitive to the conditions of the system (masses of the bars, initial radii etc.), where the velocity step had to be changed differently depending on this. For example, if the step was too large the program would skip past the 'optimal velocity', and the step would have to be 'reversed' to go in the other direction, adding to the complexity of the algorithm. If the step was too small, it would take a very long time to run. It proved difficult to formulate an algorithm which calculated the step accordingly. Complexity also arose due to the fact that both bars' radii change had to be minimised, which means that the program had to work on both velocities simultaneously. This is because changing the velocity of one bar affected the deviation in both bars. The level of 'tinkering' that this method needed to work deemed it unfavourable as a ways of minimising the ellipticities of the Bars.

It was therefore decided that the first method (2 arrays) would be revisited in a more intelligent way. Instead of creating a huge array ($100 \times 100 = 10000$ points), an initial one of (5x5 = 25 points) was instead used. The individual arrays were set so that they ranged $\pm$ 20% from the pre-calculated velocities ($\pm$ for simplicity's sake - even though it was already determined that Bar 1 would only need to increase velocity, and Bar 3 decrease). The program was ran, performing the integration of the orbits for all 25 points. To find the two corresponding velocity values which

minimised the spread of both bars, a more concrete criteria was used. Instead of looking at the velocities which minimised the value of $\sigma_{R1} + \sigma_{R3}$ (σ = Standard Deviation), the ones which minimised $\frac{R1_{Max} - R1_{Min}}{\widetilde{R1}} + \frac{R3_{Max} - R3_{Min}}{\widetilde{R3}}$ were used. Since the spread on R3 was ≈ 50 times bigger than that for R1, R1's weight in the calculation (originally) was completely insignificant - and ignored by the program. The new way gets around this by involving a fractional spread of the overall radius, whereby the two spread values for R1 and R3 will consequently become the same order of magnitude.

Once the optimal velocity combination was found, the program was repeated, except the two arrays were recreated so that they were now centered on the (just determined) pair of optimal velocities. The spread within the arrays was also decreased by a factor of two (from 20% to 10% for the second iteration) in order to 'zero in' on the correct velocities. The 25 new velocity combinations were used in the integration again to find the next set of velocities which minimised the radii deviation. This pair of velocities were set as the centre of two new arrays etc. This method was iterated many times, with the range of the arrays being decreased by a factor of two each time. This method proved successful. The below figures show the Radii of the two Bars as a function of angle, with use of the just referenced velocity correction method (25 iterations):

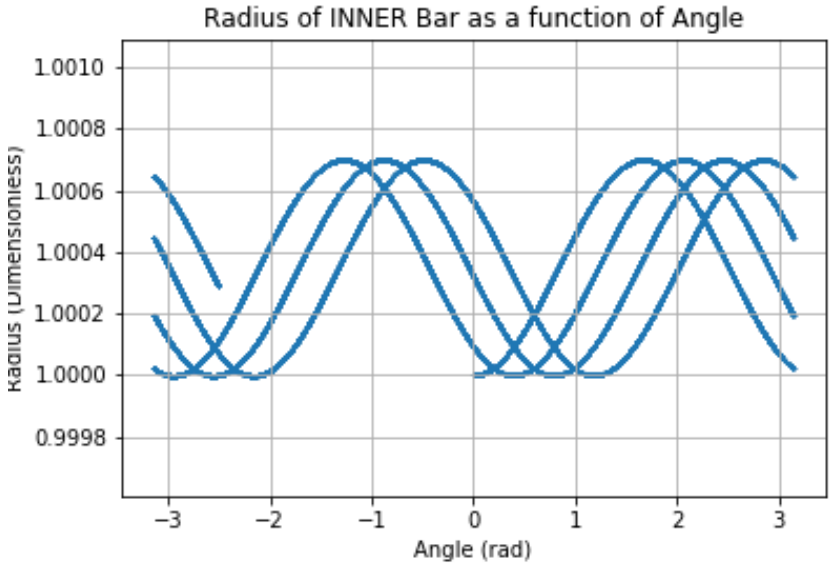

Figure 15: Radius of Inner Bar as a function of rotational angle, with fully corrected initial velocities (5 time units)

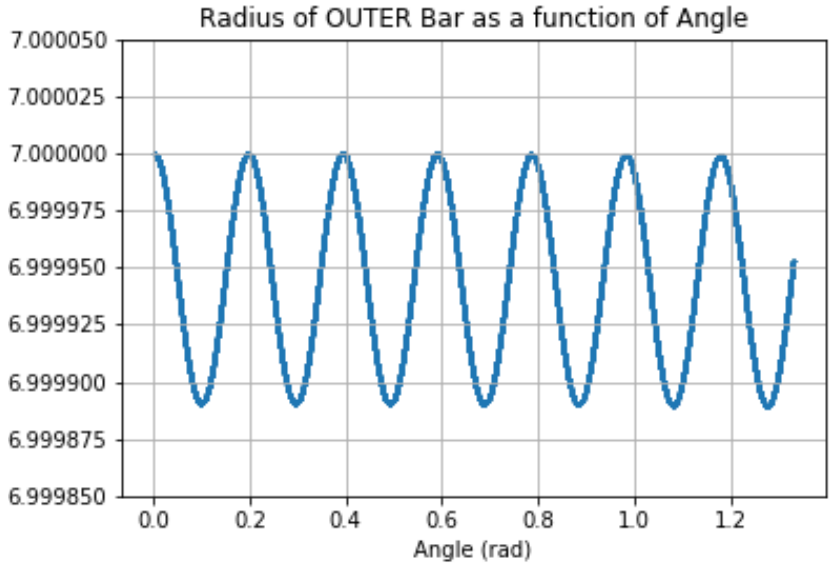

Figure 16: Radius of Outer Bar as a function of rotational angle, with fully corrected initial velocities (5 time units)

The free oscillations are now minimised, since the oscillations no longer have a 2π period (as was seen with the free oscillating Keplerian orbits previously). All that remains are the forced oscillations (the effects from the other Bar), which takes the form of a sinusoid. The Inner Bar appears to have a 'phase' - the oscillations do not follow a period related to the x-axis unit π. This is because the orbit precesses as it is influenced by the Outer Bar. This effect would be visible for the Outer Bar as well if the program was ran for a longer time (has only just reached $\theta \approx 1.2$ rad here).

2.5 Changing of Reference Frames

Once the orbits have been sufficiently circularised in the inertial frame (reference frame of the central mass), the next step is to change said reference frame so that it is fixed to both the inner bar and the outer bar (in separate instances). In these frames, the opposite bar will not have a circular orbit due to the forced oscillations. These forced oscillations should have a period of π when measured in the frame of the opposing bar. Essentially, this method will act to demonstrate how one bar affects the other. To fix the reference frame to the bar, the coordinate axes must be rotated so that it is at the same angle as the bar. This is achieved by first defining a point P in the original frame which has polar coordinates (r, α), so that:

$$x = r\cos\alpha \qquad y = r\sin\alpha \tag{33}$$

It is noted that (following convention), angles start at 0 on the positive x axis and rotate anti-clockwise until at 360° or 2π (at the start again). These angles are calculated through trigonometry, by taking the arctangent of the coordinates, for example: $\theta = arctan\left(\frac{y}{x}\right)$. In the new coordinate frame, the radius r of the point P will remain as the same value, since this is an angular matter (rotating frame). The new angle of the point P however, will be equal to the angle of the point (α), subtracted by the current rotational angle of the bar (θ), as so:

$$x' = r\cos(\alpha - \theta) = r\cos\alpha\, cos\theta + r\sin\alpha\, sin\theta$$
$$y' = r\sin(\alpha - \theta) = r\sin\alpha\, cos\theta - r\cos\alpha\, sin\theta \tag{34}$$

Where above, the standard trigonometric identities of subtraction are used:

$$\cos(x - y) = \cos x\ \cos y + \sin x\ \sin y$$
$$\sin(x - y) = \sin x\ \cos y - \cos x\ \sin y \tag{35}$$

Inputting Equation 33 into the above (Equation 34) gives:

$$x' = x\cos\theta + y\sin\theta$$
$$y' = -x\sin\theta + y\cos\theta \tag{36}$$

The coordinate of any given point in the rotating frame can now be calculated by using the original x and y coordinates of said point, along with the current angle that the reference frame bar is at (with respect to the original frame). This angle can found simply by calculating the arctangent of the coordinates of the mass on the end of the Bar in question: $\theta = arctan\left(\frac{y}{x}\right)$. This same procedure can be used to find the velocities in the new reference frame, by simply replacing x with the velocity in the x direction, and similarly for y. Shown below:

$$v_x' = v_x\cos\theta + v_y\sin\theta$$
$$v_y' = -v_x\sin\theta + v_y\cos\theta \tag{37}$$

2.6 Calculating the Angular Velocity

The results will focus on the variation in radius and angular velocity of the ends of the Bars. The radius calculation has already been visited, and goes as $r = \sqrt{x^2 + y^2}$, where the x and y coordinates are output by the program at each time-step.

To calculate the angular velocity it is slightly more difficult. It can be found through $\omega = \frac{v}{r}$, where v is the tangential velocity and r is the radius just shown. The tangential velocity is not given by the program however, only the x and y components (of the velocity). Also, since the orbits are often non circular, the tangential velocity cannot be accurately calculated through $v = \sqrt{v_x^2 + v_y^2}$, since the orbits will not necessarily be perpendicular to the radial direction to the origin. To more precisely measure the angular velocity, another form whereby $\omega = \frac{d\theta}{dt}$ is used. The change in angle per time-step, whereby $\theta = arctan(\frac{y}{x})$ can be calculated (x and y are given by the program). A numpy (Python) module called 'gradient' (https://numpy.org/doc/stable/reference/generated/numpy.gradient.html) is used whereby it returns well calculated values of the change per entry in the array (the derivative at each point). Since a great number of steps were used (50000) the gradient calculated at each point would be very accurate, being essentially indistinguishable from the 'true derivative'. This method provides a good way to work out the angular velocities of the Bars when they are undergoing non-circular motion.

2.7 Obtaining the 'Real' galaxy Parameters

As of now, a model has been created which successfully simulates the dynamic motion of a rotating Double Bar system. This model takes as input the constituent masses, their initial positions and the time to run the model for. In order to represent a real system, the real **proportions** for these parameters need to be used (as explained in section 2.1.2).

A way to determine the proportions is with use of the 'torque' which the Bars produce - these **have** been measured for Bars of different galaxy Morphologies [1]. In this particular branch of physics, 'torque' is the ratio between the tangential and radial forces that is felt by a mass lying on the Bar's orbit (forces from both the central and bar masses). Modelling and varying the masses in a Bar system (in a variation of the already created model) which has an extractable torque value, and checking if this value is equal to that which has been measured in reality, it can then be assumed that the mass proportion used in the model is the same as which was seen in the real observation. It is important to note that the known torque values are only for the primary Bar - no data is available for the secondary Bar. This is because it is much smaller and obscured, making it harder to observe. Therefore, assuming that the secondary bar act in the same way (relative to its torque) that the primary bar, the mass ratios of the inner and outer bars relative to the central mass can be calculated separately (two instances of this static model).

A good estimate for the maximum torque (maximum torques were measured in the referenced study) is when the test mass and the Bar are angularly separated by 45°. This will therefore be used in the model. The below figure displays a static model of a central mass and a bar which is on a circular orbit, which aims to help in explaining the process behind calculating this torque:

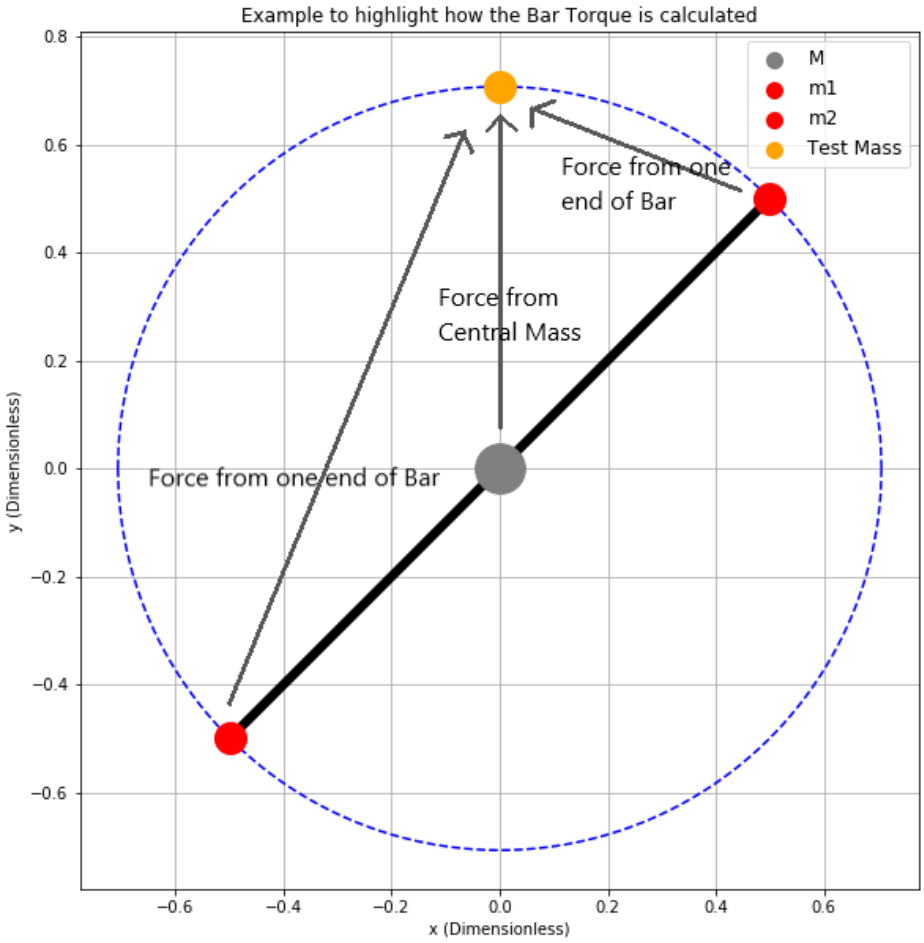

Figure 17: Example to highlight how the Bar Torque is calculated

The total tangential and radial forces felt by the test mass can respectively be calculated as the sum of these forces felt from each mass constituent (Central mass and the two ends of the Bar). Since the torque is a force ratio the mass of the (test) mass lying on the Bar's orbit' can be arbitrarily set, since it will cancel out (will be set as 1 for simplicity). The equations to find the tangential (F_T) and radial (F_R) components of each total force are provided below:

$$F_T = F_y cos\theta - F_x sin\theta \tag{38}$$

$$F_R = F_x cos\theta + F_y sin\theta \tag{39}$$

The forces are of course found with basic Newtonian gravity (Equation 1 and Equation 2). Also to note is that the angle θ is the azimuthal angle of the test mass around the origin. The torque Q is therefore defined as:

$$Q = \frac{F_y cos\theta - F_x sin\theta}{F_x cos\theta + F_y sin\theta} \tag{40}$$

As an example, a model of the Bar system with a mass ratio of 5 (Central mass is five times more massive than the Bar) gives a torque value on the test mass as $Q = 0.21$. This value is located well within the data range as referenced in [1], meaning that this method involving the torques of the Bars can reliably be used for analysis of realistic Galaxies later in this report.

3 Results and Analysis

3.1 Exploring the Parameter Space

This section intends to explore the parameter space of the created model. The space comprises of the constituent Masses of the system (Central, Inner Bar, Outer Bar), as well as the Initial Positions (Radius from origin) of the Bars. These ratios will be varied in order to investigate the behaviour of the system in different configurations. Returning to the main notion of this project, what will be focused on is the dynamic effects of the Bars on **each other** (hence the changing of reference frames) throughout this parameter space. The studied effects are the radii and angular velocity oscillations of the two Bars.

The graphs are plot in a modulus π form for ease of analysis, since the oscillations generally follow a period of π (all relevant information contained within this range). It is paramount to state that for the y axes of the plots (radius/angular velocity) the radius and angular velocity are both as measured in the **rest frame**. The x axes (angle) are as measured in each **rotating frame** of the two Bars. This is so that the notion of **when** certain effects occur relative to the opposing Bars can be studied. The reason that the angular velocity plots use a combination of the rotating (x) and rest (y) frames is because the angular velocity of one bar observed by the other will simply be the negative angular velocity of the observing bar. This is of course gives a low potential for analysis. In the rest frames, the angular velocities of the bars have full freedom to be as disparate as possible. The radius is measured the same in the rest or rotating frame so it does not matter which version is plot. The time period that the graphs are represented over are relatively arbitrary, having been set so that a sufficient amount of data can be extracted, but not too long that the program takes too long to run. They are referenced in the captions of their specific figure.

The parameters will be varied by decreasing one particular value until the model either reaches its limits by becoming unstable, or when sufficient data has been acquired to notice a clear trend in the data. The process of variation will take the following form: start with the 'safe' parameters which were used in the **method** section; reduce the central mass M until the model meets its limits; reduce the mass of the Inner Bar until the model meets its limits; reduce the radius of the Outer Bar until the model meets its limits. The succeeding section 3.2 will delve into the details of why the model meets its 'limits', and what this looks like.

3.1.1 Varying the Central Mass

Below, shown are the plots for the Radii and Angular Velocities of each Bar (in each frame). The blue (left) plots denote the radius oscillations and the red (right) plots denote the angular velocity oscillations. The top row of plots gives data for the Inner Bar whereas the bottom row gives data

for the Outer Bar. The first overall set of plots use the example (safe) parameters which were being utilised throughout the **method** section (Central Mass = 20). Plots are then further provided whereby the central mass is decreased to 10, 5, 1, 10^{-10} and 10^{-50} respectively.

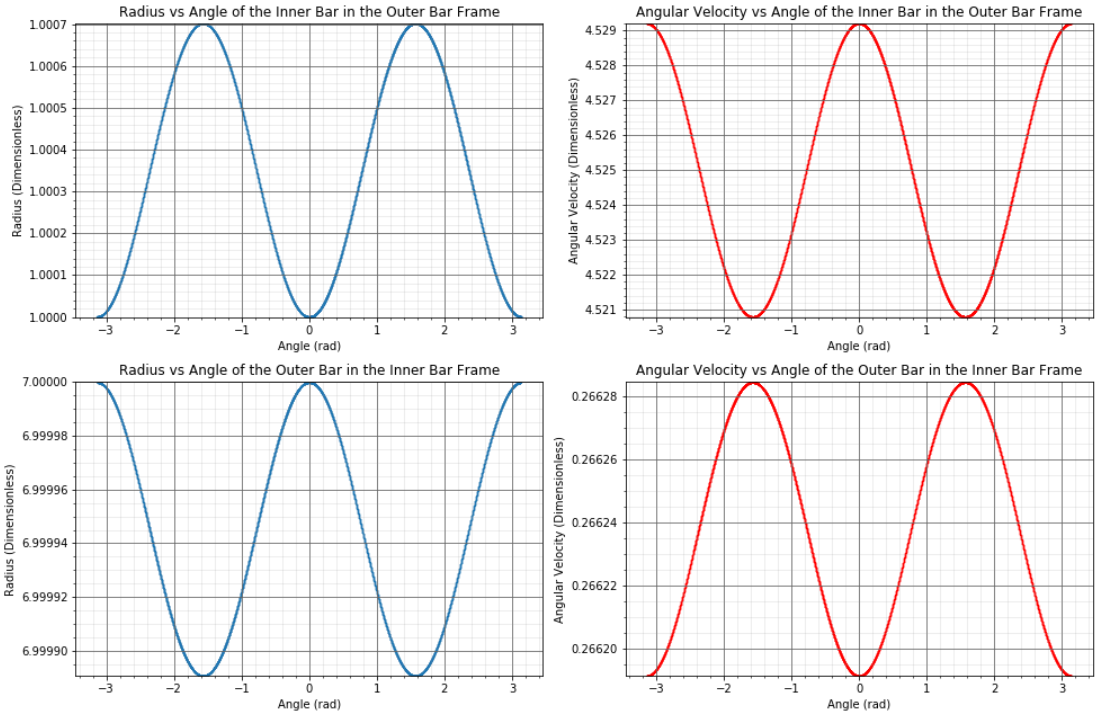

Figure 18: Radius and Angular Velocity Results: **Central Mass = 20**, Inner Bar Mass = 4, Outer Bar Mass = 2; Inner Bar Initial Radius = 1, Outer Bar Initial Radius = 7; (Time = 5)

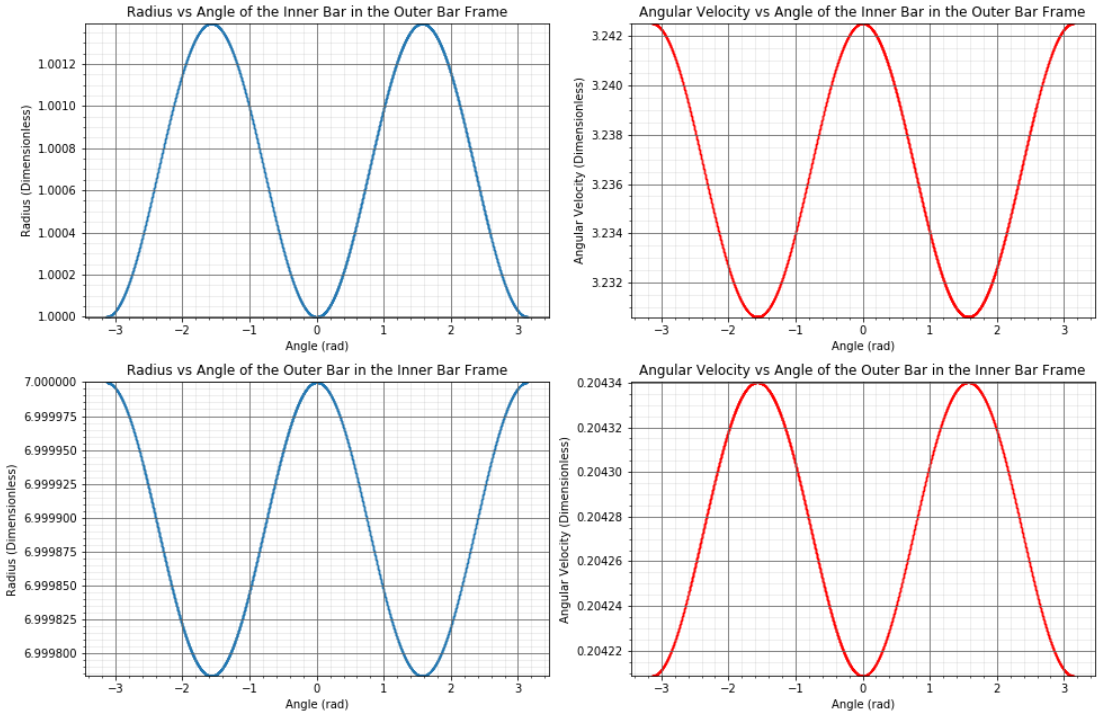

Figure 19: Radius and Angular Velocity Results: **Central Mass = 10**, Inner Bar Mass = 4, Outer Bar Mass = 2; Inner Bar Initial Radius = 1, Outer Bar Initial Radius = 7; (Time = 5)

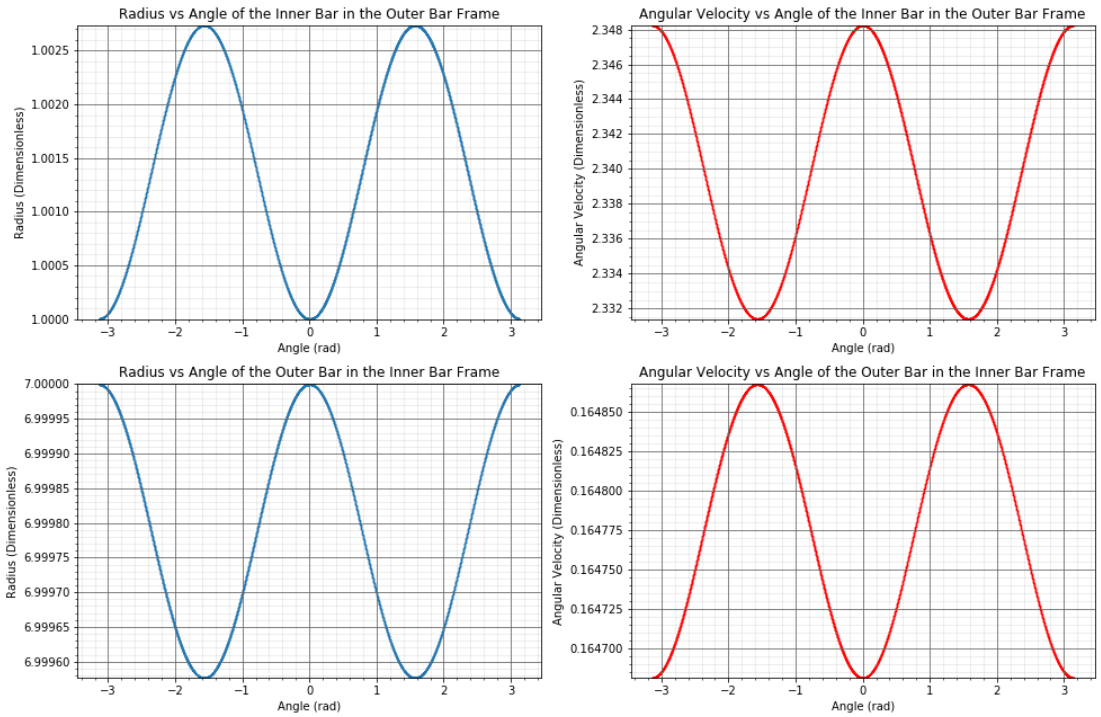

Figure 20: Radius and Angular Velocity Results: **Central Mass = 5**, Inner Bar Mass = 4, Outer Bar Mass = 2; Inner Bar Initial Radius = 1, Outer Bar Initial Radius = 7; (Time = 10)

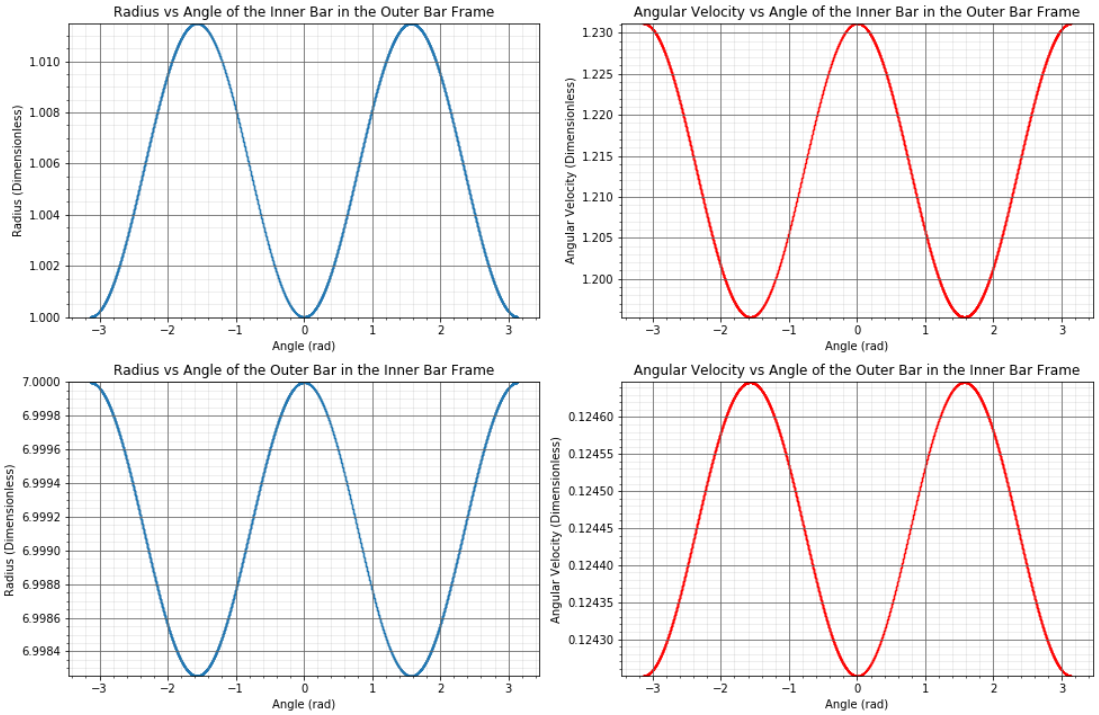

Figure 21: Radius and Angular Velocity Results: **Central Mass = 1**, Inner Bar Mass = 4, Outer Bar Mass = 2; Inner Bar Initial Radius = 1, Outer Bar Initial Radius = 7; (Time = 10)

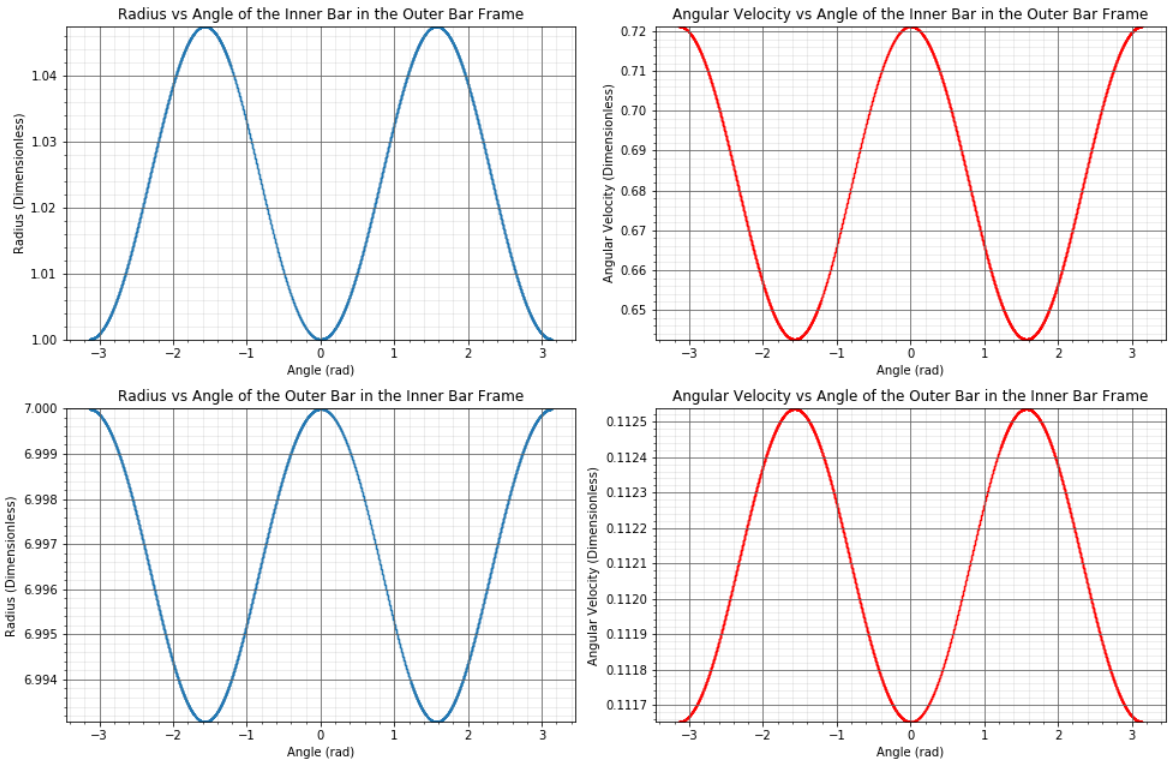

Figure 22: Radius and Angular Velocity Results: **Central Mass =** 10^{-10}, Inner Bar Mass = 4, Outer Bar Mass = 2; Inner Bar Initial Radius = 1, Outer Bar Initial Radius = 7; (Time = 20)

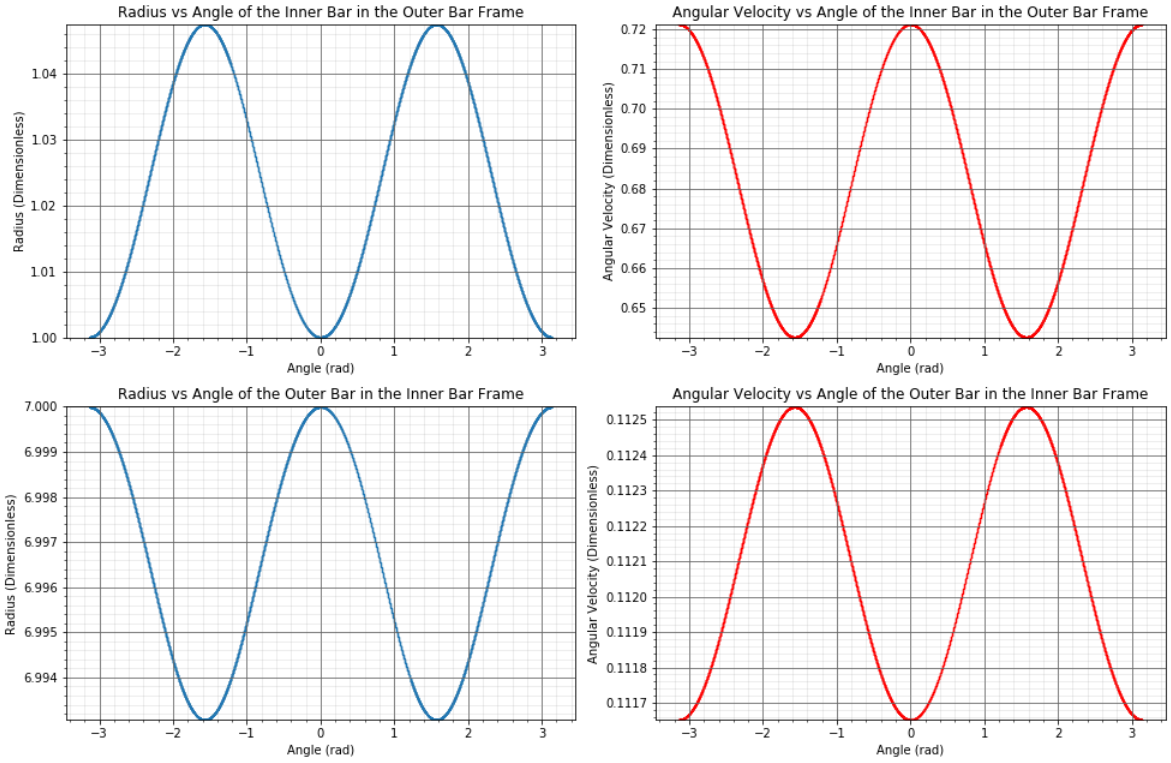

Figure 23: Radius and Angular Velocity Results: **Central Mass =** 10^{-50}, Inner Bar Mass = 4, Outer Bar Mass = 2; Inner Bar Initial Radius = 1, Outer Bar Initial Radius = 7; (Time = 20)

The overall amplitudes of all of these plots are tabulated below for ease of analysis later on. Also included is a relative amplitude for each oscillation, which represents how much the oscillation (peak/trough) deviates from its average value (middle). The amplitudes within these tables are further arranged as plots, in terms of each subsequent table entry as the mass is changed i.e. How the radius and angular velocity amplitudes of the two bars change as mass is varied. The plots will be displayed in either a linear or log-log fashion based on what will be suitable, given the group of results.

Table 2: Radii Amplitudes of the Inner and Outer Bars as the Central Mass is varied (Inner Bar Mass = 4, Outer Bar Mass = 2; Inner Bar Initial Radius = 1, Outer Bar Initial Radius = 7)

Central Mass	Inner Bar Radius Amplitude	Inner Bar Relative Radius Amplitude	Outer Bar Radius Amplitude	Outer Bar Relative Radius Amplitude
20	3.51×10^{-4}	0.035 %	5.45×10^{-5}	0.0005 %
10	6.95×10^{-4}	0.070 %	1.08×10^{-4}	0.001 %
5	1.37×10^{-3}	0.15 %	2.12×10^{-4}	0.0025 %
1	5.75×10^{-3}	0.60 %	8.75×10^{-4}	0.0125 %
10^{-10}	2.38×10^{-2}	2.45 %	6.34×10^{-3}	0.05 %
10^{-50}	2.38×10^{-2}	2.45 %	6.34×10^{-3}	0.05 %

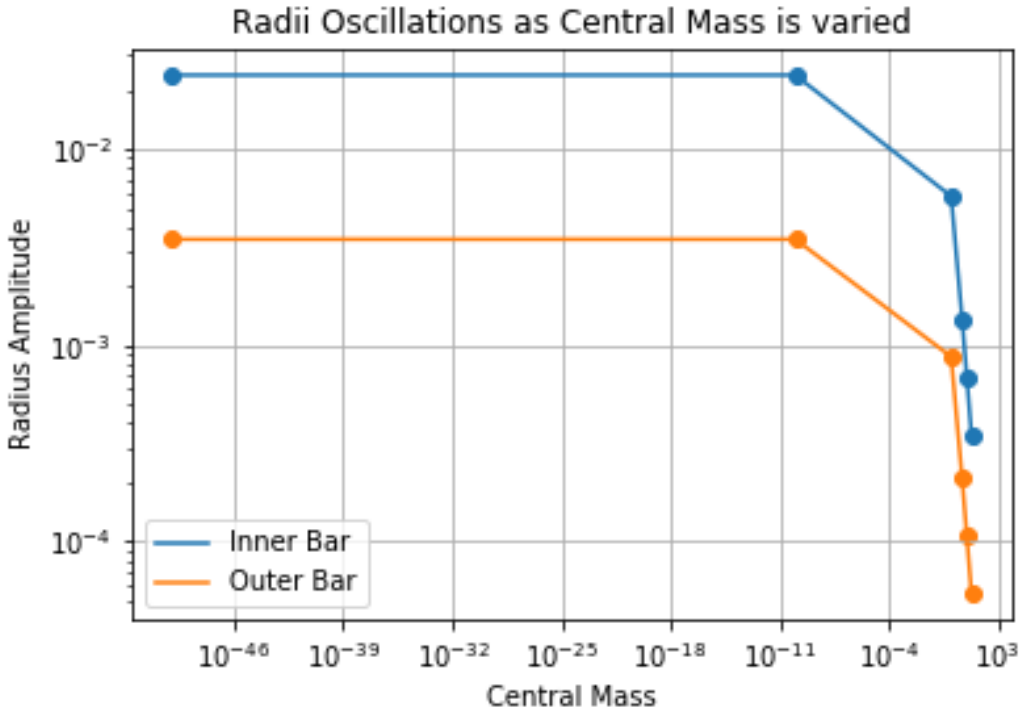

Figure 24: Radius Oscillation Amplitudes as the Central Mass is varied

Table 3: Angular Velocity Amplitudes of the Inner and Outer Bars as the Central Mass is varied (Inner Bar Mass = 4, Outer Bar Mass = 2; Inner Bar Initial Radius = 1, Outer Bar Initial Radius = 7)

Central Mass	Inner Bar Angular Velocity Amplitude	Inner Bar Relative Angular Velocity Amplitude	Outer Bar Angular Velocity Amplitude	Outer Bar Relative Angular Velocity Amplitude
20	4.21×10^{-3}	0.09 %,	4.62×10^{-5}	0.019 %
10	5.95×10^{-3}	0.19 %	6.60×10^{-5}	0.035 %
5	8.40×10^{-3}	0.34 %	9.30×10^{-5}	0.060 %
1	1.79×10^{-2}	1.44 %	1.99×10^{-4}	0.16 %
10^{-10}	3.94×10^{-2}	5.88 %	4.43×10^{-4}	0.40 %
10^{-50}	3.94×10^{-2}	5.88 %	4.43×10^{-4}	0.40 %

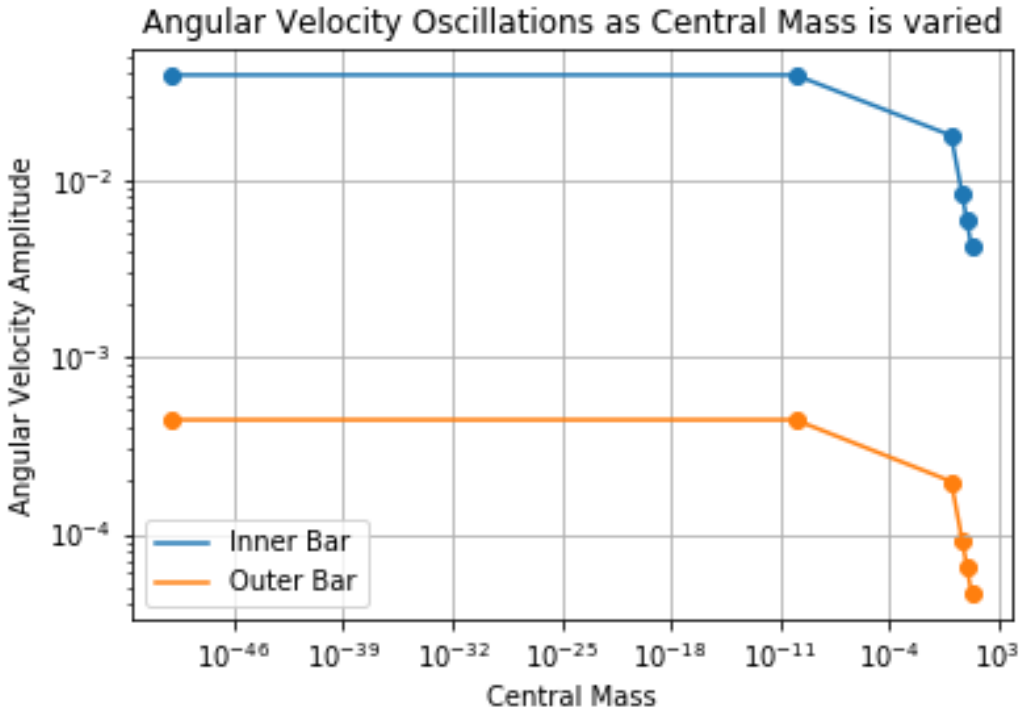

Figure 25: Angular Velocity Oscillation Amplitudes as the Central Mass is varied

3.1.2 Varying the Inner Bar Mass

With the effects of the Central Mass on the fixed oscillations of the system (Radius and Angular Velocity) having been detailed, what shall be studied next is how the mass of the **Inner Bar** affects the oscillations within the system. Following the same structure as before, plots are provided below for Inner Bar Masses 2, 1, 0.1 and 0.01 respectively. To investigate the oscillations better, the Central Mass is valued as $M = 1$ (lower mass so more visible interactions between the Bars). It is not defined too low (10^{-10} for example) because then it will most likely have no effect on the system at all. The other parameters (initial radii, Outer Bar mass) stay as they were before.

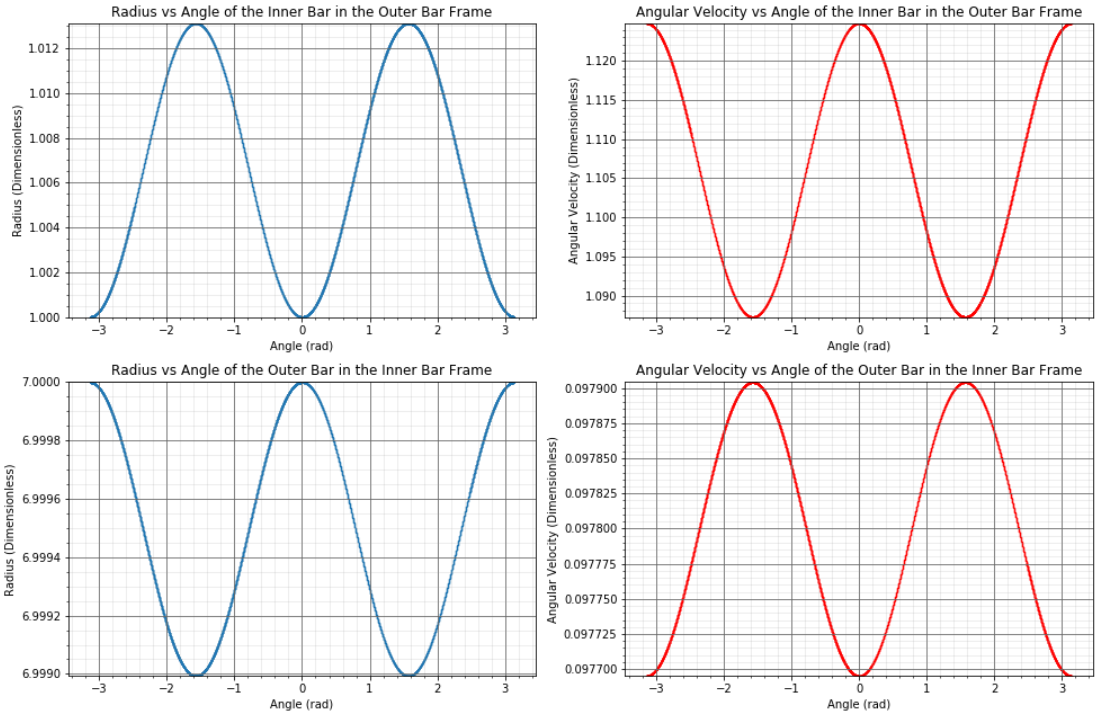

Figure 26: Radius and Angular Velocity Results: Central Mass = 1, **Inner Bar Mass = 2**, Outer Bar Mass = 2; Inner Bar Initial Radius = 1, Outer Bar Initial Radius = 7; (Time = 10)

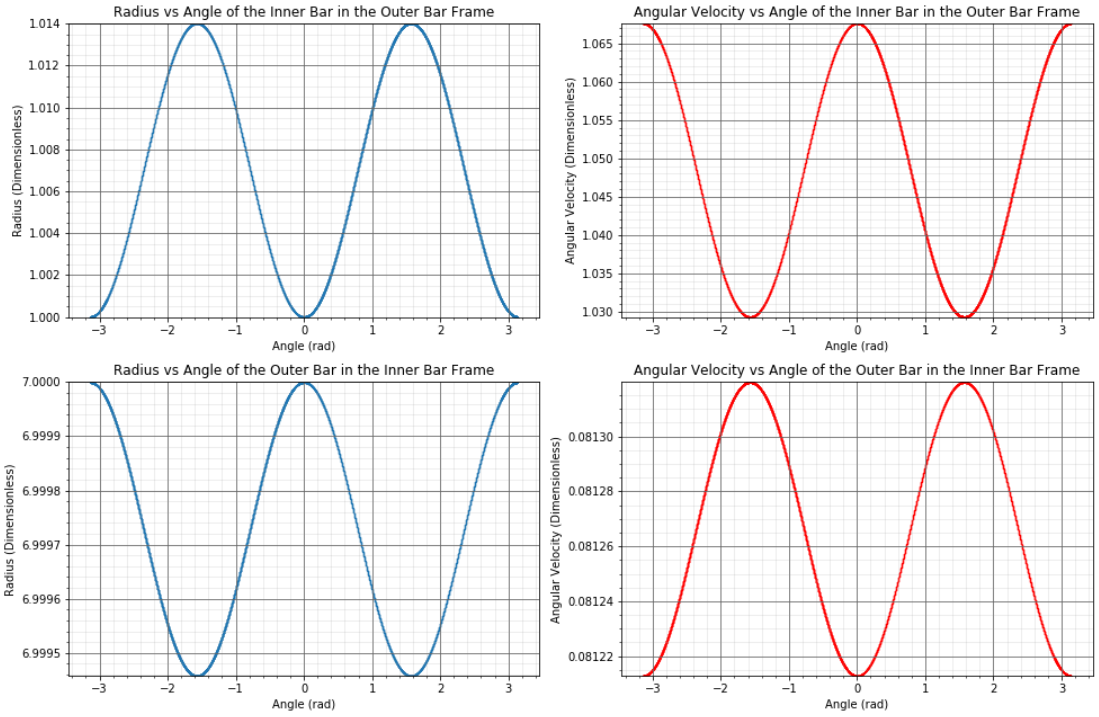

Figure 27: Radius and Angular Velocity Results: Central Mass = 1, **Inner Bar Mass = 1**, Outer Bar Mass = 2; Inner Bar Initial Radius = 1, Outer Bar Initial Radius = 7; (Time = 10)

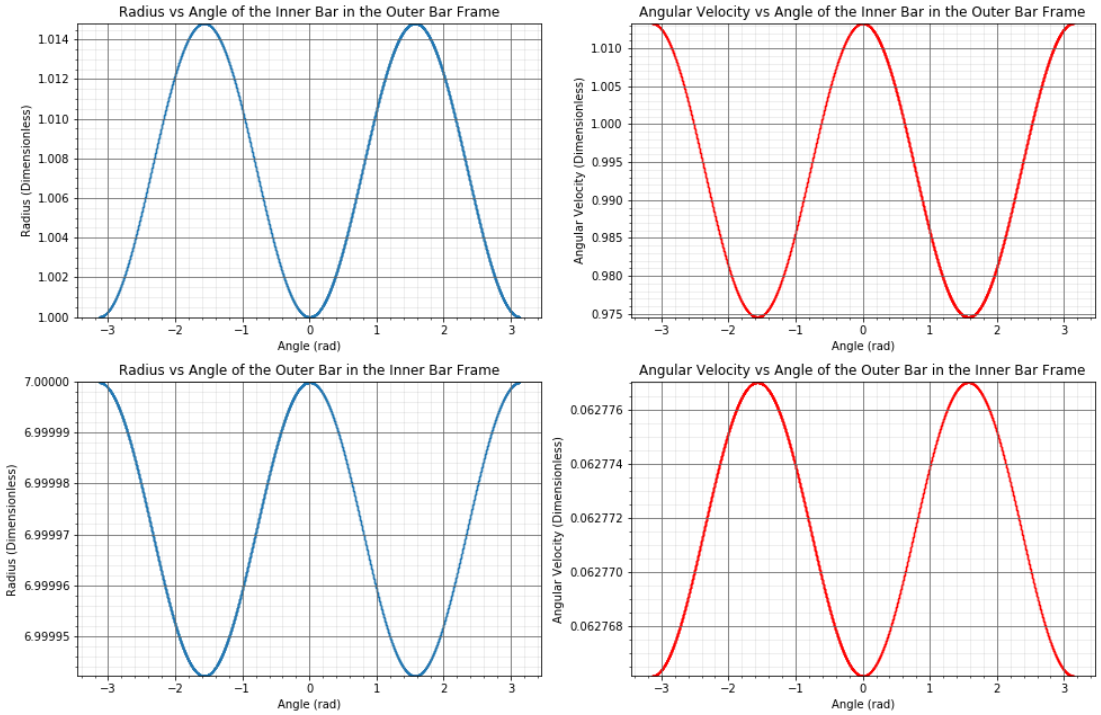

Figure 28: Radius and Angular Velocity Results: Central Mass = 1, **Inner Bar Mass = 0.1**, Outer Bar Mass = 2; Inner Bar Initial Radius = 1, Outer Bar Initial Radius = 7; (Time = 10)

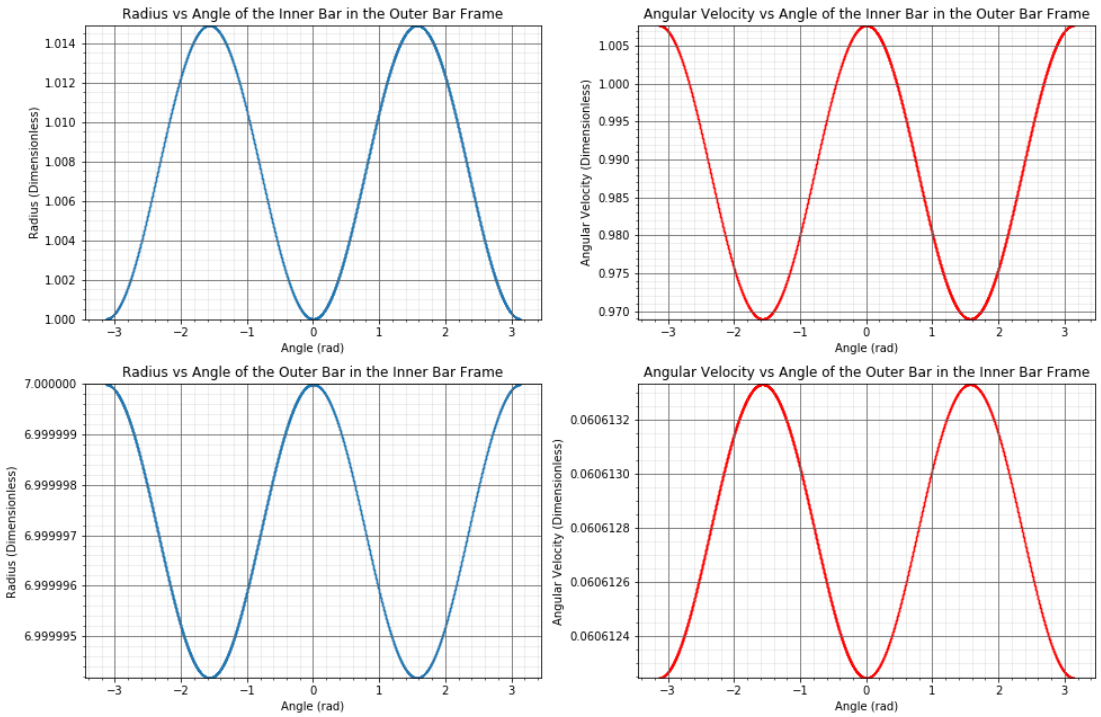

Figure 29: Radius and Angular Velocity Results: Central Mass = 1, **Inner Bar Mass = 0.01**, Outer Bar Mass = 2; Inner Bar Initial Radius = 1, Outer Bar Initial Radius = 7; (Time = 10)

Again, these results are tabulated below, in terms of the amplitude change per figure. Further plots are then provided based on these amplitudes.

Table 4: Radii Amplitudes of the Inner and Outer Bars as the Inner Bar Mass is varied (Central Mass = 1, Outer Bar Mass = 2; Inner Bar Initial Radius = 1, Outer Bar Initial Radius = 7)

Inner Bar Mass	Inner Bar Radius Amplitude	Inner Bar Relative Radius Amplitude	Outer Bar Radius Amplitude	Outer Bar Relative Radius Amplitude
2	6.55×10^{-3}	0.69%	5.05×10^{-4}	0.0070 %
1	7.00×10^{-3}	0.70%	2.72×10^{-4}	0.0043 %
0.1	7.40×10^{-3}	0.80 %	2.90×10^{-5}	0.00043 %
0.01	7.50×10^{-3}	0.80 %	2.92×10^{-6}	0.000043 %

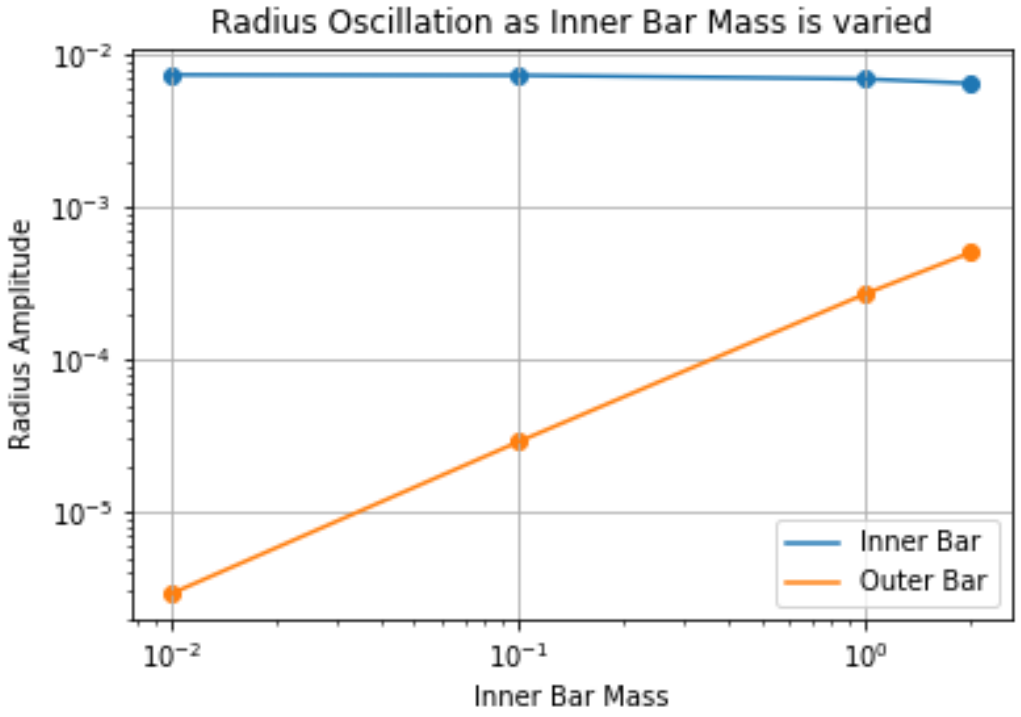

Figure 30: Radius Oscillation Amplitudes as the Initial Outer Bar Distance is varied

Table 5: Angular Velocity Amplitudes of the Inner and Outer Bars as the Inner Bar Mass is varied (Central Mass = 1, Outer Bar Mass = 2; Inner Bar Initial Radius = 1, Outer Bar Initial Radius = 7)

Inner Bar Mass	Inner Bar Angular Velocity Amplitude	Inner Bar Relative Angular Velocity Amplitude	Outer Bar Angular Velocity Amplitude	Outer Bar Relative Angular Velocity Amplitude
2	1.88×10^{-2}	1.81 %	1.05×10^{-4}	0.10 %
1	1.92×10^{-2}	1.91 %	5.35×10^{-5}	0.08 %
0.1	1.94×10^{-2}	2.01 %	5.40×10^{-6}	0.01 %
0.01	1.94×10^{-2}	2.03 %	5.45×10^{-7}	0.001 %

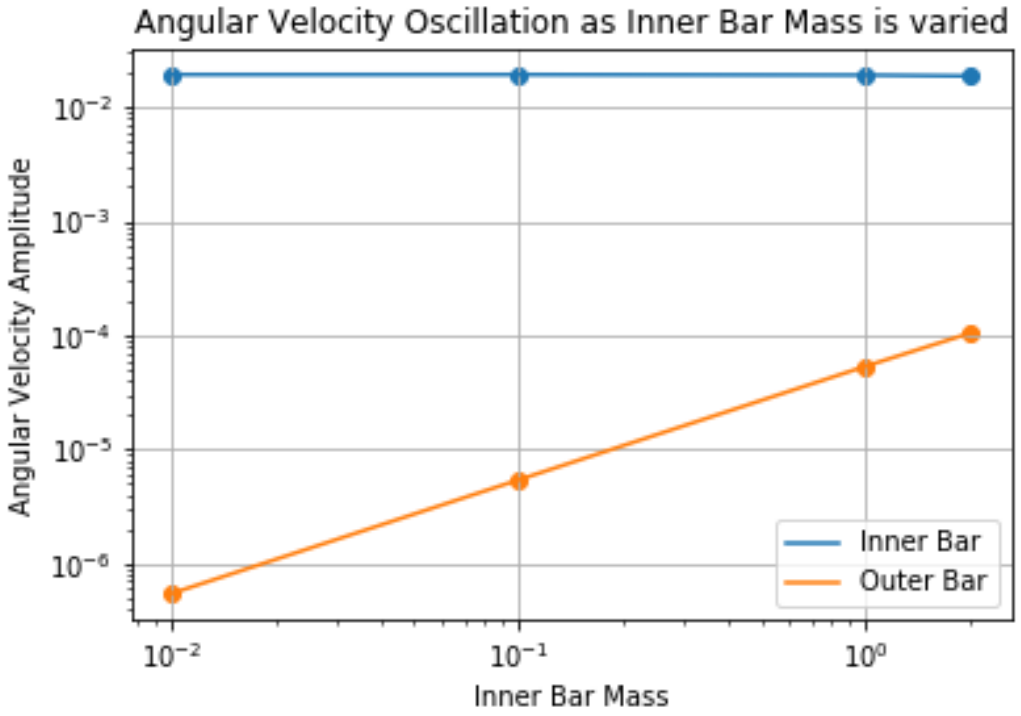

Figure 31: Angular Velocity Oscillation Amplitudes as the Inner Bar Mass is varied

3.1.3 Varying the Outer Bar Initial Radius

The effects of the mass values of the systems have now been detailed (Central and Inner Bar Mass). It is not necessary to change/investigate the Outer Bar's mass since it will most likely cause the same effect that changing the Inner Bar's does (albeit just in the opposite way). The effects that the Initial Positions of the Bars have on the system now need to detailed. Below, plots where the initial radius of the Outer Bar is varied are shown. It is set as 6, 5, 4, 3 and 2.875 respectively. The Central mass is set relatively high, at 5. This is to keep the system stable. For the same reason, the Inner and Outer Bar masses are set as 4 and 2 respectively. The Initial Radius of the Inner

Bar is kept at 1, as before.

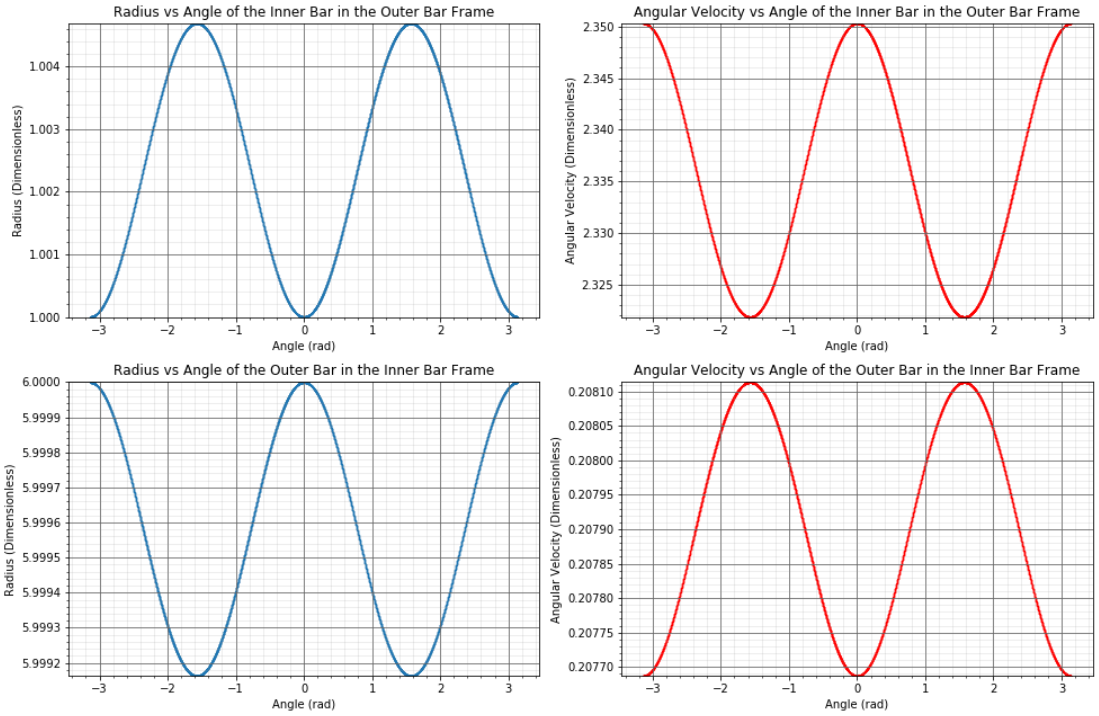

Figure 32: Radius and Angular Velocity Results: Central Mass = 5, Inner Bar Mass = 4, Outer Bar Mass = 2; Inner Bar Initial Radius = 1, **Outer Bar Initial Radius = 6**; (Time = 10)

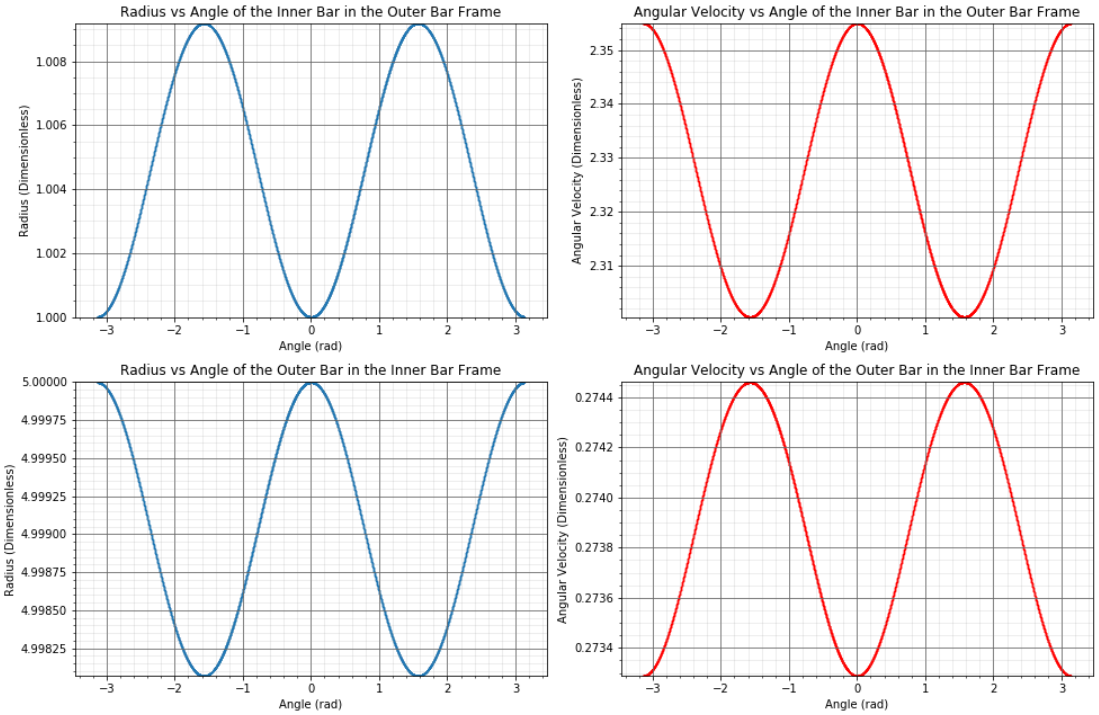

Figure 33: Radius and Angular Velocity Results: Central Mass = 5, Inner Bar Mass = 4, Outer Bar Mass = 2; Inner Bar Initial Radius = 1, **Outer Bar Initial Radius = 5**; (Time = 10)

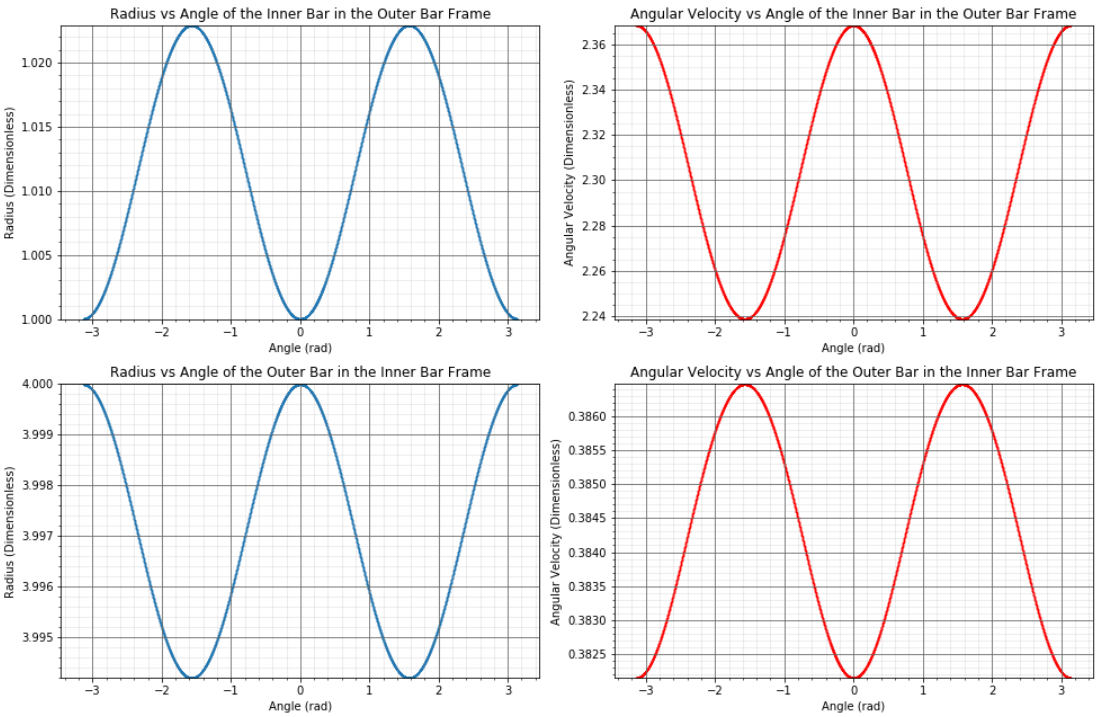

Figure 34: Radius and Angular Velocity Results: Central Mass = 5, Inner Bar Mass = 4, Outer Bar Mass = 2; Inner Bar Initial Radius = 1, **Outer Bar Initial Radius = 4**; (Time = 10)

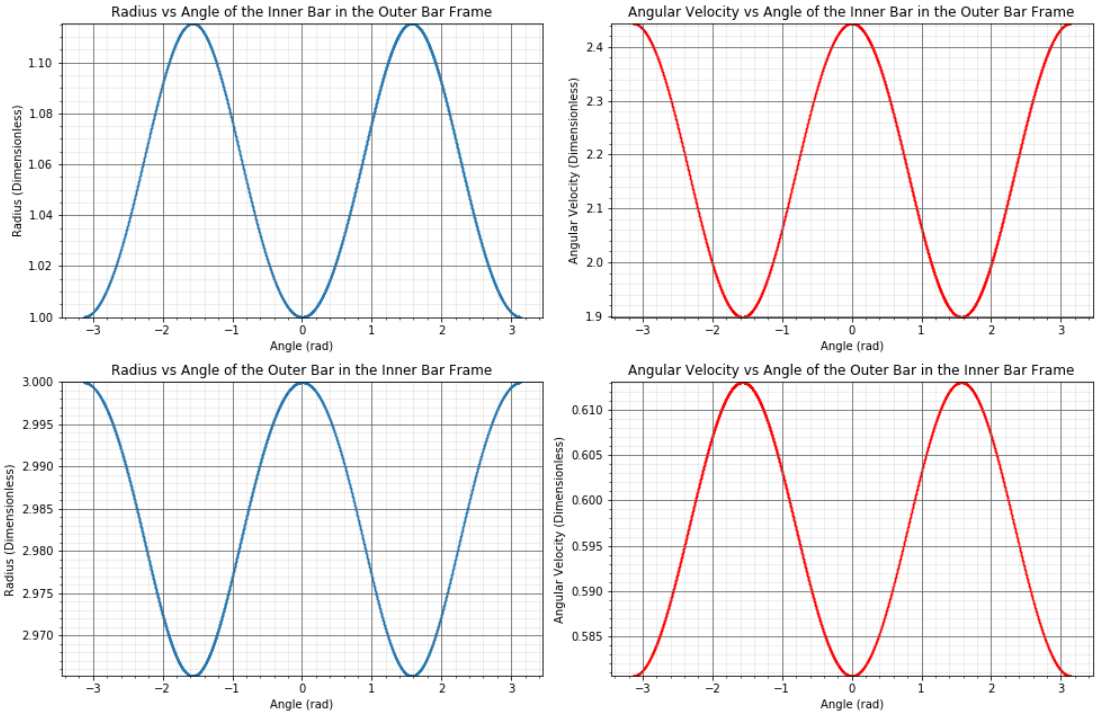

Figure 35: Radius and Angular Velocity Results: Central Mass = 5, Inner Bar Mass = 4, Outer Bar Mass = 2; Inner Bar Initial Radius = 1, **Outer Bar Initial Radius = 3**; (Time = 10)

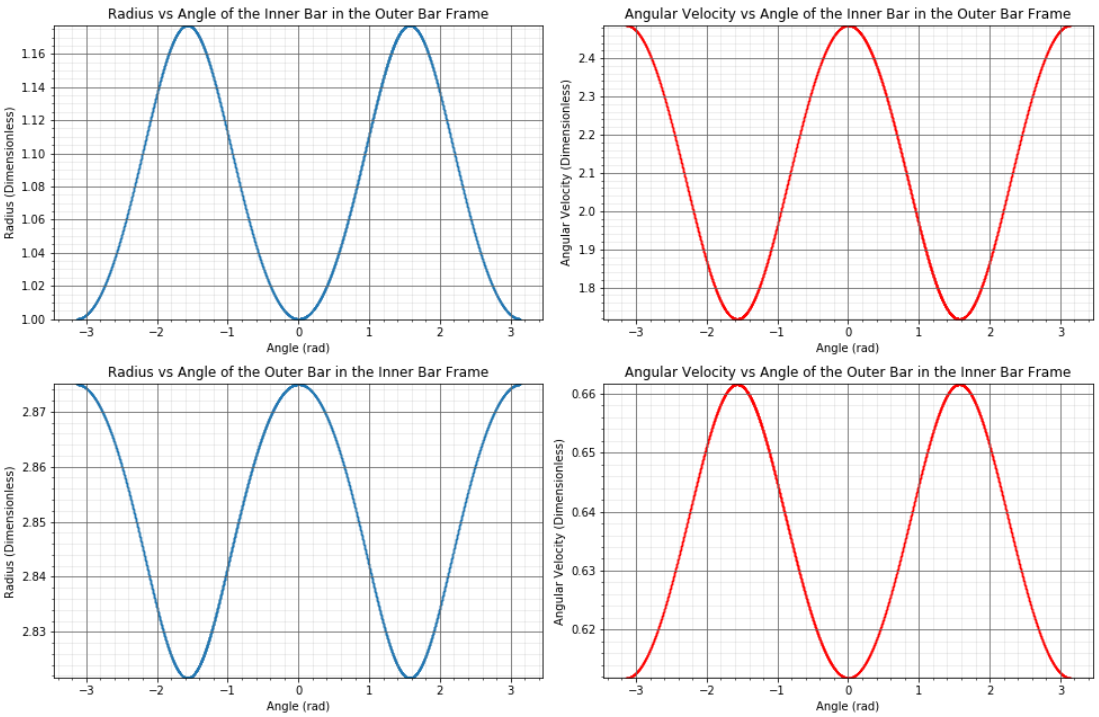

Figure 36: Radius and Angular Velocity Results: Central Mass = 5, Inner Bar Mass = 4, Outer Bar Mass = 2; Inner Bar Initial Radius = 1, **Outer Bar Initial Radius = 2.875**; (Time = 10)

The amplitudes of these figures are further tabulated and plot below:

Table 6: Radii Amplitudes of the Inner and Outer Bars as the Outer Bar Initial Distance is varied (Central Mass = 5, Inner Bar Mass = 4, Outer Bar Mass = 2, Inner Bar Initial Radius = 1)

Outer Bar Initial Radius	Inner Bar Radius Amplitude	Inner Bar Relative Radius Amplitude	Outer Bar Radius Amplitude	Outer Bar Relative Radius Amplitude
6	2.35×10^{-3}	0.25 %	4.20×10^{-4}	0.0065 %
5	4.60×10^{-3}	0.45 %	9.70×10^{-3}	0.020 %
4	1.15×10^{-2}	1.24 %	2.90×10^{-3}	0.075 %
3	5.80×10^{-2}	5.72 %	1.74×10^{-2}	0.59 %
2.875	8.87×10^{-2}	8.26 %	2.67×10^{-2}	0.96 %

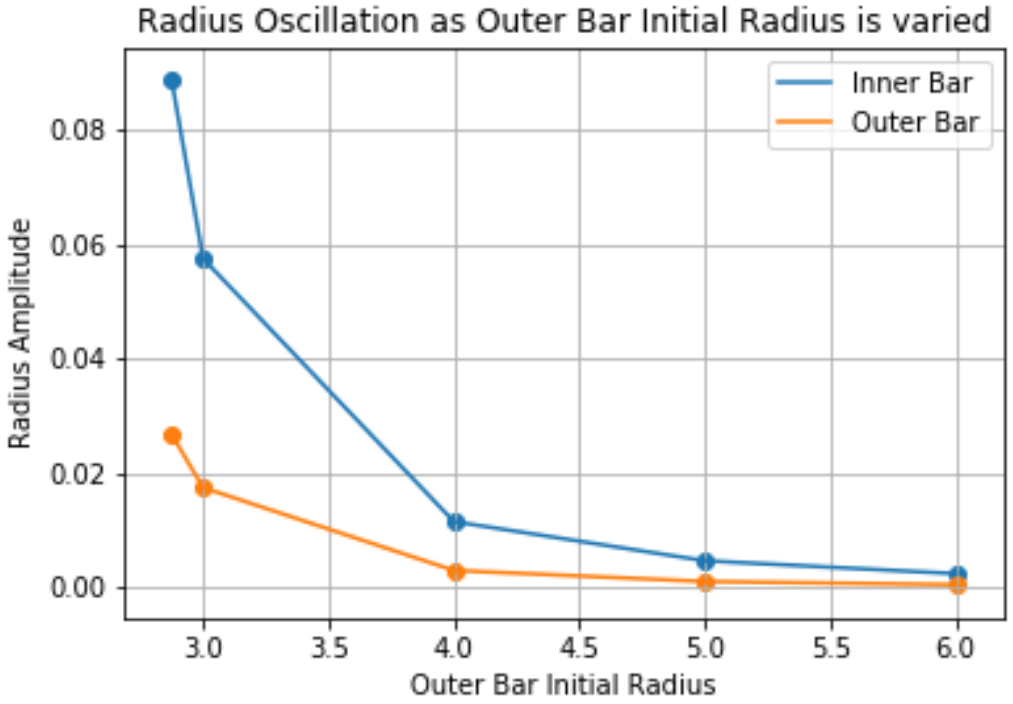

Figure 37: Radius Oscillation Amplitudes as the Initial Outer Bar Distance is varied

Table 7: Angular Velocity Amplitudes of the Inner and Outer Bars as the Outer Bar Initial Distance is varied (Central Mass = 5, Inner Bar Mass = 4, Outer Bar Mass = 2, Inner Bar Initial Radius = 1)

Outer Bar Initial Radius	Inner Bar Angular Velocity Amplitude	Inner Bar Relative Angular Velocity Amplitude	Outer Bar Angular Velocity Amplitude	Outer Bar Relative Angular Velocity Amplitude
6	1.43×10^{-2}	0.64 %	2.14×10^{-4}	0.10 %
5	2.73×10^{-2}	1.29 %	5.85×10^{-4}	0.22 %
4	6.50×10^{-2}	2.83 %	2.17×10^{-3}	0.59 %
3	2.73×10^{-1}	12.79 %	1.62×10^{-2}	2.93 %
2.875	3.84×10^{-1}	19.05 %	2.49×10^{-2}	4.06 %

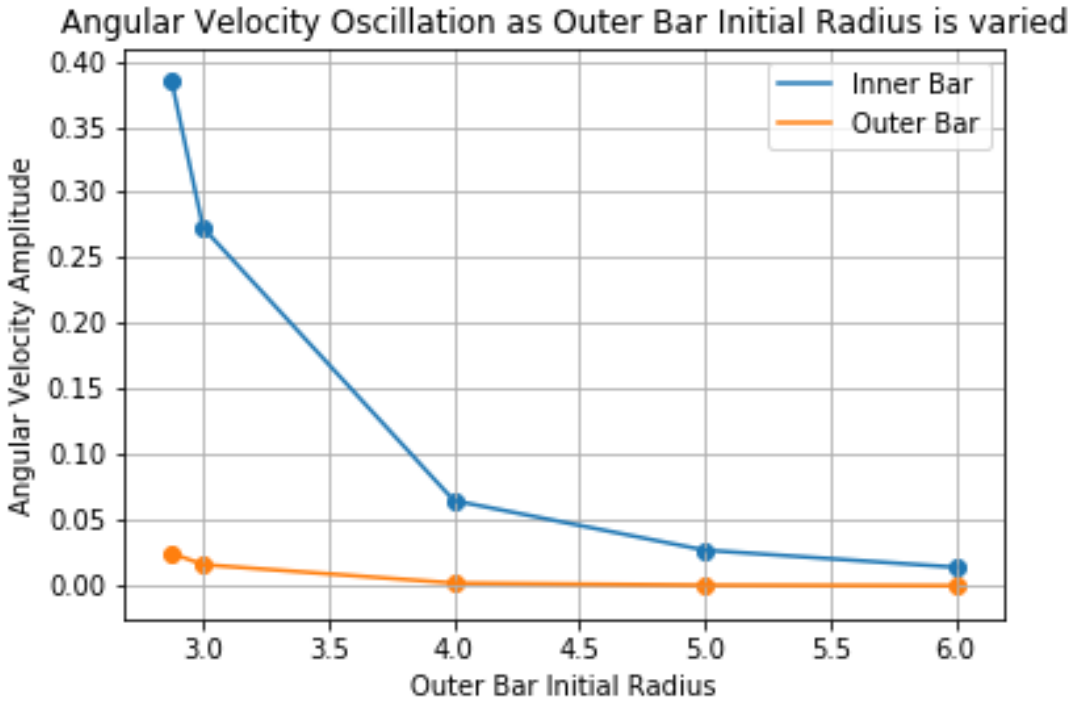

Figure 38: Angular Velocity Oscillation Amplitudes as the Initial Outer Bar Distance is varied

3.2 Other Results

In the section of this project whereby the parameter space was explored 3.1, there were specific limits which the model could be pushed to. These observed limits comprised of the initial radii and masses of the Bars. Once the values passed certain thresholds the system behaved in a manner which was not desired (non sinusoidal oscillations). In this section, plots are shown for where the system acted in this 'undesired' way.

3.2.1 Chaotic Motion

First, plots are shown below for where the Outer Bar radius is reduced to **2**. This acted as a continuation from the data in section 3.1.3, where the outer bar initial radius was decreased from to 6, 5, 4 and then 3.

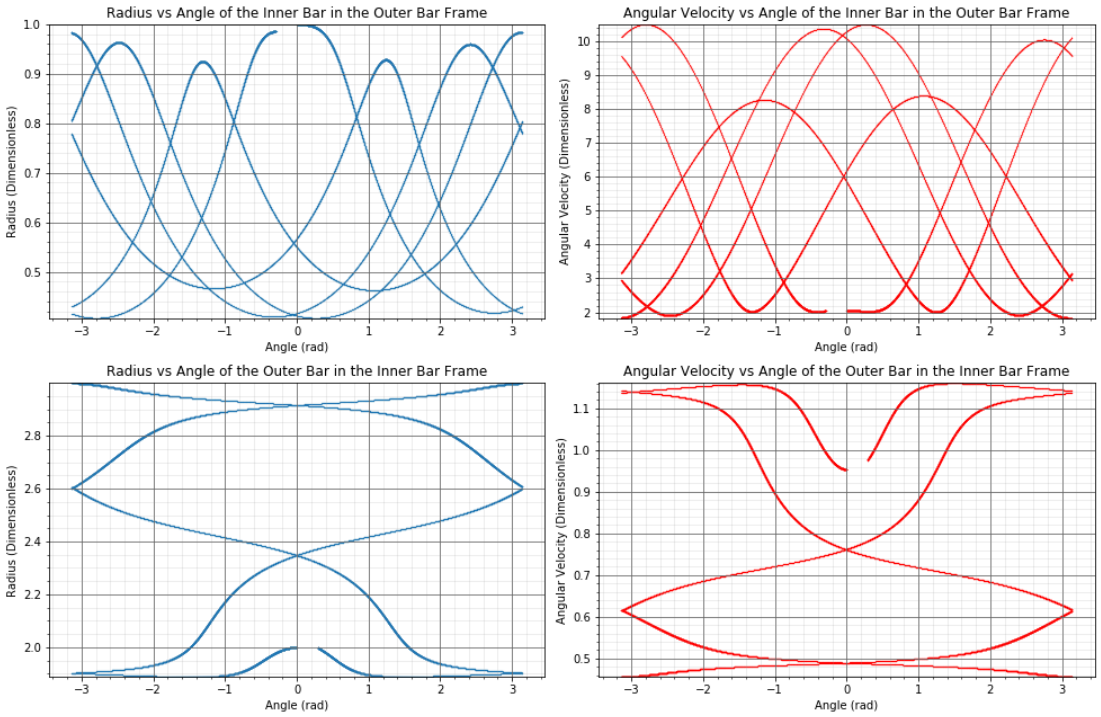

Figure 39: Radius and Angular Velocity Results: Central Mass = 1, Inner Bar Mass = 2, Outer Bar Mass = 2; Inner Bar Initial Radius = 1, **Outer Bar Initial Radius = 2**; (Time = 10)

3.2.2 Inconsistent Periods

Certain parameter combinations were found to give more stable orbits than the system just mentioned, however they still did not display periodicity which would have been expected for a system of this type. For example, if **both** the Central and Inner Bar Masses, as well as the Outer Bar Initial Radius were decreased at the same time (From the spaces of which stable values were found) plots such as those below were output:

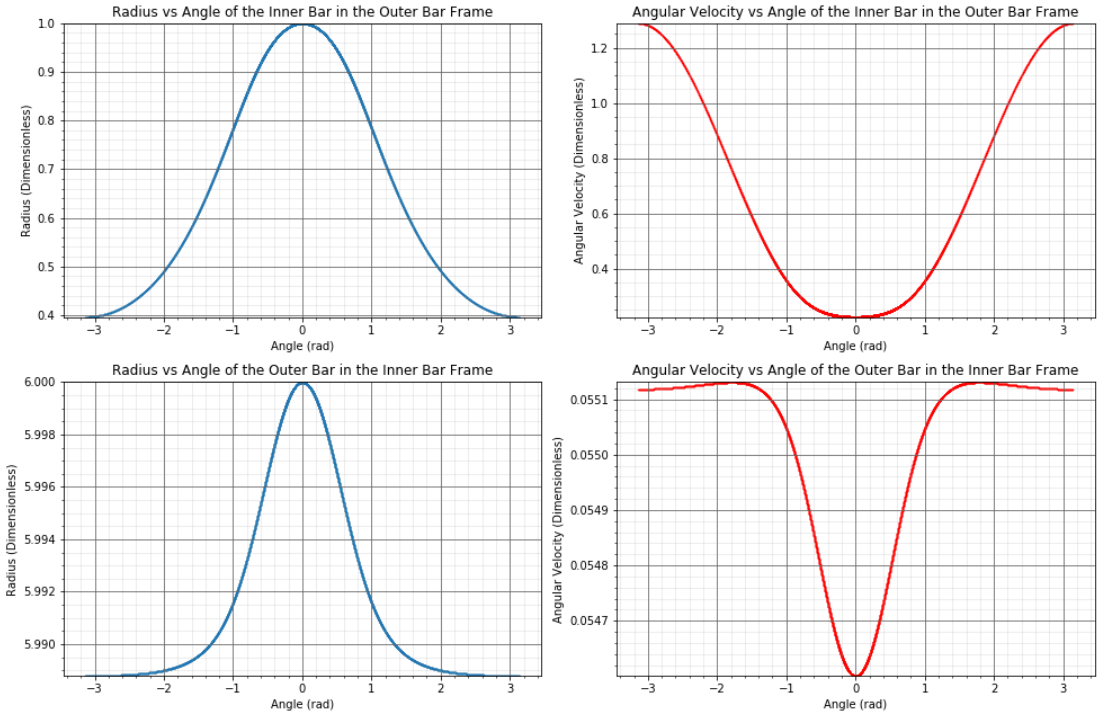

Figure 40: Radius and Angular Velocity Results: **Central Mass = 0.01**, **Inner Bar Mass = 0.5**, Outer Bar Mass = 1; Inner Bar Initial Radius = 1, **Outer Bar Initial Radius = 6**; (Time = 50)

3.2.3 Near Stable

For another example of where the program is unable to return pure fixed oscillations, a particular configuration of the model whereby the system is very near the edge of stability (by our definitions of uniform π period oscillations) is shown below.

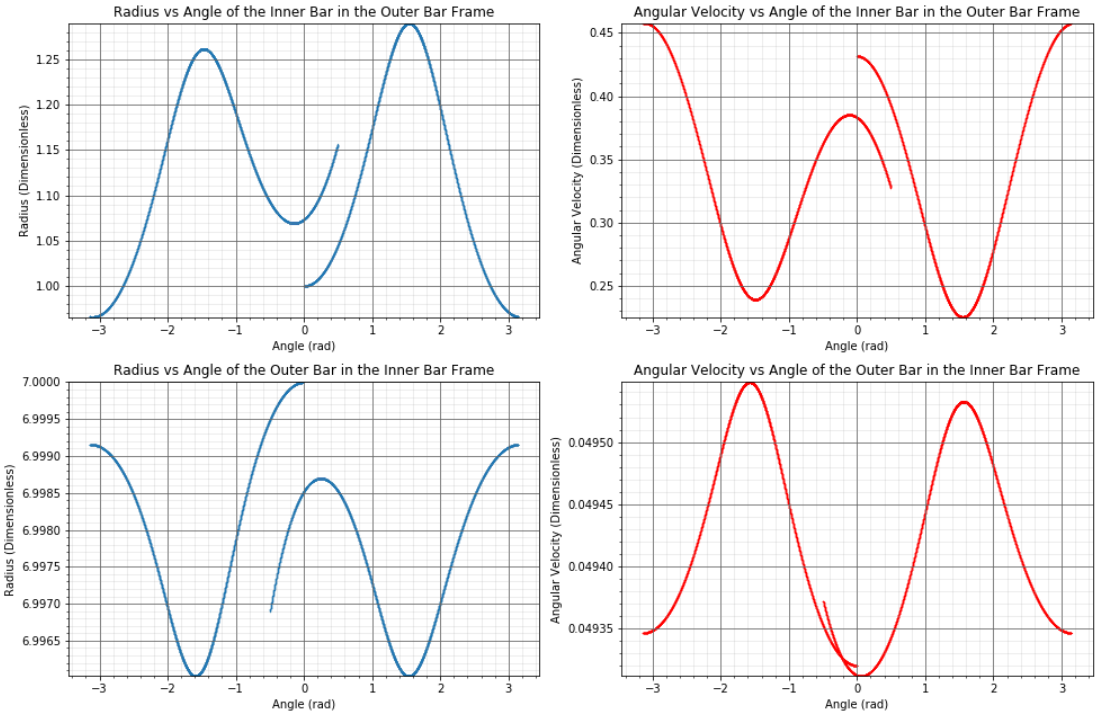

Figure 41: Radius and Angular Velocity Results: Central Mass = 0.1, Inner Bar Mass = 0.4, Outer Bar Mass = 2.7; Inner Bar Initial Radius = 1, Outer Bar Initial Radius = 6; (Time = 25)

4 Discussion

As can be clearly seen, the general oscillation plots all follow a sinusoidal pattern as expected, with a clear oscillatory period of π throughout. Firstly, the overall shape of the plots shall be analysed. This applies to all of the plots since they only vary in amplitude - their overall angular characteristics (angle of max/min etc.) are equivalent.

Focusing on the **Inner Bar's** Radius plot for this analysis (top left of all general oscillation figures), it is clear that the radius of the Bar is minimum at angles 0 and π, and maximum at $\pm\frac{\pi}{2}$. Since these graphs are in the angular reference frame of the other rotating Bar, this means that the radius is minimum when the Bars are aligned and maximum when perpendicular. Conversely, the angular velocity plots for the **Inner Bar** (top right of all figures) trend in the opposite way (minimum at angles $\pm\frac{\pi}{2}$, and maximum at 0 and π), meaning that the angular velocity is maximum when the Bars are aligned and minimum when they are perpendicular.

The below figures aim to highlight these orientations, whereby the left graph shows the Bars in parallel alignment and the right shows them in perpendicular alignment. Only one end of each Bar is coloured. This is to highlight how one end of the binary mirrors the other end, meaning that only one end needs to be studied for results.

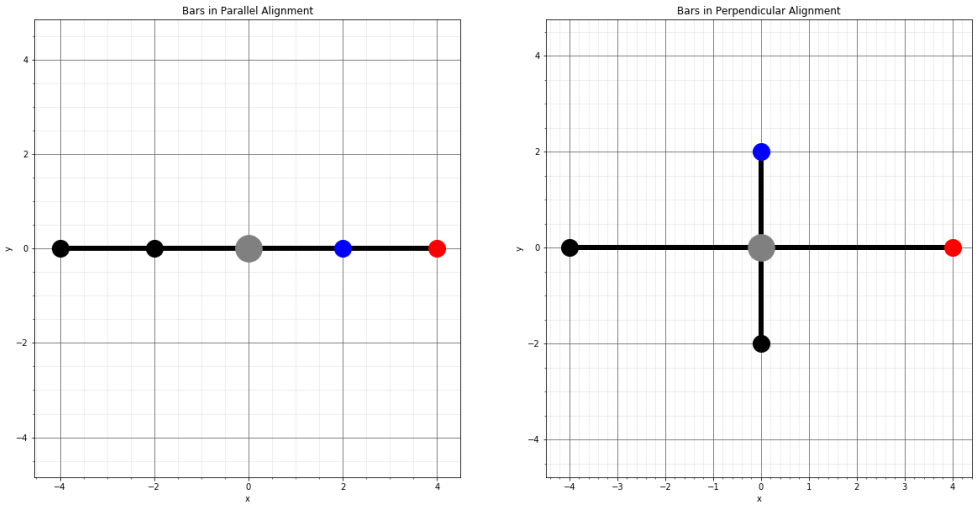

Figure 42: Parallel/Perpendicular Alignment Demonstration

What is the reason for this effect, whereby the Inner Bar's radius increases/angular velocity decreases, as the Bars fall out of alignment? This is a consequence of the unstable/stable equilibrium nature of the two respective configurations just referenced (parallel/perpendicular). Consider the parallel aligned configuration (first figure), whereby $t = 0$ and $\theta = 0$ since the Bars are started off in alignment. The system is in a stable position here because the forces all propagate upon one single axis (x-axis). As the Inner Bar (blue) rotates anti-clockwise, the Outer Bar (red) gravitationally pulls the Inner Bar towards it, in an effort to bring it back to the equilibrium axis. As it does this, a natural consequence is that the Inner Bar (blue) will reduce in angular velocity (it is travelling away from the Outer Bar and so will be slowed down). Due to the conservation of angular momentum, this means that the radius must increase to compensate for the reduction in velocity. This effect continues (radius/angular velocity keeps increasing/decreasing) until the system hits its turning point, whereby the Bars are perpendicularly aligned at $\theta = \frac{\pi}{2}$ (second figure). Once past this point, the dominant force felt by the Inner Bar (blue mass) due to the Outer Bar switches from the red mass to the black mass which is on the other side. This is because it has passed the y-axis and so is now closer to the other end. Since the Inner Bar is now travelling **towards** the Outer Bar (x-axis), it will instead now be accelerated, since the force is in the direction of travel. This increases the angular velocity and therefore decreases radius (conservation of angular momentum). This will carry on until the Inner Bar is at $\theta = \pi$, whereby the Bars have now returned to the parallel alignment configuration, allowing this whole process to be repeated again.

Looking at the figures for the **Outer Bar's** radius and angular velocity over time (bottom left and right of all the general oscillation plots), the same effect which the Inner Bar experiences is seen, albeit in the inverse direction. This is because (starting from the parallel aligned configuration), as the Inner Bar rotates away from the Outer Bar, it exerts gravitational force upon the Outer Bar which 'drags' it along (in the direction of its movement), thus increasing its angular velocity. This will of course reduce the radius due to the conservation of angular momentum. Again, this effect will reverse once the Bars have moved past perpendicular alignment, since the closest mass changes to the one which is on the other side of the other bar. This is located in the opposite relative direction

as the other side of the Bar was, and so it will decrease the angular velocity, and increase the radius.

Looking at the specific values for the maxima and minima of the radius plots for both Bars, it is clear that the initially set radius value for the Inner Bar acts as its **minimum** point, whereas the initially set radius value for the Outer Bar acts as its **maximum** point. Referring to the previous analysis, this makes sense since the Inner Bar is only going to oscillate 'outwards' from its starting position due to the influence of the Outer Bar. Of course, this entails that the Outer Bar will only oscillate 'inwards' from its starting position, due to the influence of the Inner Bar.

4.1 Varying the Central Mass - Results Section 3.1.1

In terms of the amplitudes of the radii oscillations for each Bar (blue), they both increase as the central mass is lowered from its starting value of 20, to 10, 5, 1, 10^{-10} and then to 10^{-50}. The reason for the collective increase is that the central mass's influence is lessened as it decreases in mass, due to Newton's law of Gravitation (Force decreases linearly). Since the central influence decreases, but the other Bar's influence stays the same, the proportion of force felt from the other Bar (as a function of total force) will increase. The central mass works to keep the orbits circular - and therefore radii constant (free oscillations minimised). The other Bar however works to cause oscillatory movement (forced oscillations), which of course will be made more prominent if its influence increases (as seen in the results).

A noticeable characteristic of the radii amplitudes is that the Inner Bar's are ≈ 10 times greater for each studied system (varying central mass). It was difficult to pinpoint a reason for this, but a potential reason is that since the Outer Bar is further out than the Inner Bar, it can approximate the Inner Bar and Central Mass as one object (at least better than the Inner Bar can). This leaves it as a two body problem, where perfectly circular orbits can be attained (0 amplitude). This is a potential explanation for why the oscillations of the Outer Bar are smaller than that of the Inner Bar.

As expected, the amplitude of the angular velocity oscillations increase as the central mass is decreased, due to the proportional relationship between radius and angular velocity (radius amplitude is seen to increase as shown in the radius table table). The previous analysis explaining why this amplitude increases (for the radii) holds the same weight here i.e. The central mass has less of an influence which allows the forced oscillations to grow in size (bigger amplitudes).

The previously touched upon notion, whereby (at each central mass entry) the Inner Bar amplitudes are greater than that of the Outer Bar, is even more pronounced for the angular velocities. The Inner Bar has overall oscillation amplitudes which are ≈ 100 times greater than that of the Outer Bar (at each central mass entry), compared to the radii amplitudes where this value was only ≈ 10. Since the radius and angular velocity are linked, it is understandable that the angular velocity will experience a similar effect as before (seen with the radii values), whereby the Outer Bar can better approximate the central mass and inner bar as a single object, granting less oscillatory motion. The reason why this difference has grown (from ≈ 10 to ≈ 100) is most likely due to the 'compounding effect' of there being a radius amplitude difference (as seen before), but also now a velocity amplitude difference as a result (e.g. radius increases, velocity decreases). Importantly, this velocity difference goes as $v \propto \sqrt{r}$ (basic circular motion). Since $\omega = \frac{v}{r}$, this means that the angular velocity spread goes as $\omega \propto \frac{1}{\sqrt{r}}$. This reciprocal square root means that the angular velocity amplitude differences between the Bars (for each mass entry) will be even greater than those seen

for the radial amplitudes.

With exploration, it was in fact discovered that the central mass can essentially be decreased indefinitely (in this parameter configuration), with the system still staying stable. This effect was studied by using extremely small central mass values (10^{-10} and 10^{-50}). As can be seen from the graphs, the oscillations for the extreme low mass cases show the same shape as seen for the other (much greater) mass values, showing that the system was able to reach stability by minimising the free oscillations. At this point in fact, the central mass is so small that it essentially has no effect on the Bars. This is most easily seen in the **amplitude** plots, where as the central mass is decreased the oscillations reach a limit whereby they do not increase anymore (flat line). The reason that the system can still remain stable when the mass is reduced so much is a consequence of the central mass being fixed at the origin. If the central mass was not fixed to the origin, it would instantaneously fly out of place due to the asymmetry of the system. With a negligible central mass, what is essentially occurring now is a double Binary system of the Bars which operate about their Barycenter (the origin). This system is interestingly able to stay stable, most likely as a consequence of the binary mirroring (one end of the Bar mimics the other). If this rule was not in place the system would likely fall out of stability immediately. This would be due to both the lack of a large stabilising mass in the centre, as well as the different forces that one end of the Bar would feel compared to the other end, since the Bars now don't have to be directly opposite each other (e.g. one Inner Bar end is closer to the Outer Bar than the other).

4.2 Varying the Inner Bar Mass - Results Section 3.1.2

Interestingly, as the Inner Bar's mass is decreased, the radial amplitude for the Inner Bar increases relatively slowly, whereas that for the Outer Bar decreases rather drastically in comparison. Between the first and last data points of Inner Bar mass 2 and 0.01, the Inner Bar oscillates ≈ 1.14 times bigger, whereas the Outer Bar oscillates ≈ 173 times smaller.

A clear reason for why the Outer Bar oscillations reduce is due to basic Newtonian gravity - if the mass of the Inner Bar reduces, the Outer Bar will feel a smaller force and therefore move inwards less. This change in force (and therefore oscillation) is linear ($F \propto m$) as a function of mass. This can be highlighted through the change in oscillation between adjacent data points. For example, when the mass is reduced by a factor of two from 2 to 1, the amplitude changes by $\frac{2.72\times10^{-4}}{5.05\times10^{-4}} = 0.54 \approx 0.5$. When the mass is reduced by a factor of 10 from 0.1 to 0.01, the amplitude changes by $\frac{2.92\times10^{-6}}{2.90\times10^{-5}} = 0.1007 \approx 0.1$. This shows a **linear relationship** between the mass of the Inner Bar and the oscillation amplitude of the Outer Bar, as they both change at the same rate. This effect can also be clearly seen in the plot of radii oscillations, whereby the Outer Bar line (orange) is straight.

The Inner Bar's amplitude most likely increases because the Outer Bar has more influence over it (mass ratio moves in favour of Outer Bar), and so it is able to pull it outwards further. This effect is relatively small however (compared to the change seen for the Outer Bar), which is likely due to the inverse square effect and the relative distance that the Inner Bar is to the Outer Bar and the Central Mass. Since the Inner Bar is ~ 7 times closer to the Central Mass ($7^2 = 49$ more force proportionately) than the Outer Bar, it has a greater influence over it and is able to slow down the increase in radius amplitudes (oscillations).

Regarding the angular velocity amplitude changes, the previous analysis in the central mass variation section still applies 3.1.1 - due to the proportional link between radius and angular velocity amplitude i.e since the Outer Bar's radius oscillates less, its angular velocity must also oscillate less. Conversely, since the Inner Bar's radius oscillates more (slightly), its angular velocity must also oscillate more (slightly).

4.3 Varying the Outer Bar Initial Radius - Results Section 3.1.3

Reducing the initial radius of the Outer Bar clearly increases the amplitude of oscillation for the radii and angular velocities of both the Inner and Outer Bars. This was as expected, since if the Bars are initialised closer they will feel a greater force ($\propto \frac{1}{r^2}$). This greater force means that the Bars will influence each other to a greater extent, increasing their radii change.

Interestingly, there is an 'acceleration' in the increase of the radii amplitudes as the initial radius of the Outer Bar is decreased, whereby the change between each subsequent data point increases. This effect is better comprehended in terms of a figure (Figure 37). A clear $\frac{1}{r^2}$ type effect is seen here. The force felt increases non-linearly as the distance between the Bars is decreased. This is because the overall fractional change in distance between the two Bars increases as the Outer Bar radius is decreased. For example (assuming the Inner Bar is at $r = 1$), for the first two data points whereby the Outer Bar radius is 6 and 5 respectively, Fractional Distance Change $= \frac{(6-1)-(5-1)}{6-1} = 0.20$, whereas for where the Outer Bar radius is 4 and 3, Fractional Distance Change $= \frac{(4-1)-(3-1)}{4-1} = 0.33$. This greater change in the initial radius value for the closer radii combines with the fact that the distance is squared, producing a large increase in force. This explains why the amplitudes increase greatly as the Outer Bar's radii is decreased. It also explains why the initial radius of the Outer Bar cannot be decreased any further without encountering a high level of instability, since the oscillations grow uncontrollably as the Bars are initially set closer and closer together. This is clearly shown as the vertical asymptote just below the value of 2.875 (for the initial radius) in Figure 37. When models were ran which had an outer bar initial radius valued less than the position of this asymptote, the oscillations were too high for the program to handle. It was unable to find perfectly sinusoidal varying orbits of the Bars.

With regards to the angular velocities, the same relations as seen before (with the radii) are observed i.e. as the radii amplitudes increase so do those for the angular velocities. The angular velocity amplitudes will consequently increase more-so since a higher range of orbital sizes will give rise to a greater spread in orbital velocities. Therefore since $\omega = \frac{v}{r}$, the spread in ω will increase more relative to the radii increase. It has previously been explained why this occurs in 3.1.1.

4.4 Other Results

4.4.1 Chaotic Motion - Results Section 3.2.1

The Bars are clearly no longer following simple oscillations and are varying rather irregularly. Remnants of a sinusoidal shape can be seen in the graphs for the Inner Bar, but the peaks vary in both height and width. This is because, as explained in the previous section 4.3, the oscillations of the bars grow exponentially as the distance between them is decreased. At a certain point (once less than ≈ 2.875) the velocity corrector algorithm is unable to find a velocity combination for the Bars which provide clear, stable sinusoidal oscillations (this unstable model uses an initial radius of the outer bar as 2). An initial radius for the outer bar of ≈ 2.875 therefore stands as the near

final point at which the program can find stable orbits. Of course, the initial radius value could be continuously decreased at very small increments in order to try and stay in a stable region, but this is not needed because the trend is already understood. There are **two** main reasons for its failure:

- The algorithm attempts to reduce the free oscillations by finding the velocities combination which minimises the difference between the maximum and minimum radius value. The problem with this is that it completely ignores the 'shape' of the radius plot (sinusoidal wanted) and ultimately, it assumes that the system with the purest case of fixed oscillation possible is one where the radius deviation is the least. In reality, a solution may exist for this system which gives purely sinusoidal oscillations, except it will have a relatively high value for the total radius range (deviation). Essentially, the algoritm is chasing false solution
- Since the radius deviation of **both** Bars was to be minimised, what had to be considered (and minimised) was the sum of the spreads of the Inner and Outer Bars. To negate the effect of one Bar deviating much more than the other and dominating the sum, a condition was used where the sum of fractional radius variations was minimised ie: $\frac{R1_{Max}-R1_{Min}}{\bar{R1}} + \frac{R3_{Max}-R3_{Min}}{\bar{R3}}$. The problem here however, is that it assumes that the Bar's oscillation is proportional solely to its mean radius, when in reality it is more complicated i.e It depends on the masses of the system too. This means that the program may tend to favour the minimisation of one Bar compared to another.

In a more extensive investigation, these two processes just mentioned can be altered in order to allow the model to make use of more chaotic parameters. A more specific 'sinusoidal finder' algorithm could be created, whereby it explicitly searches for solutions which follow a sinusoidal shape, opposed to just minimising the overall spread of the radius and not focusing on the shape itself. This could be achieved by (with the Inner Bar for example) searching for solutions which hold minimums at 0 and $\pm 2\pi$, and maximums at $\pm\frac{\pi}{2}$. This will naturally help to give the shape of a sinusoid since these are the conditions for one, with the added benefit of not adding any constraints on the overall amplitudes (maximum deviation) of the oscillations.

The sums of the deviations of the two Bars could also be more intelligently/complexly constructed, taking account of the constituent masses of the system as well as the radii of the two Bars. This will help to place less bias on minimising the free oscillations of one Bar compared to another.

4.4.2 Inconsistent Periods - Results Section 3.2.2

Clearly, the orbits are much more stable but strangely show only a single peak in both radius and angular velocity throughout each period of 2π (Two peaks were seen before). This is unexpected because (based on previous logic) the bars would oscillate inwards and outwards twice per relative rotation to each other, due to the fact that there are two ends to each Bar (as one end of the Bar loses its gravitational influence on the other Bar, the other end will begin to gain it). What can be assumed from these findings is that the velocity correction algorithm is unable to find a solution which gives the π periodicity as seen in the previous results (for example Figure 32). This could be either because the solution does not exist, or that the algorithm is not best equipped to find it. For the latter reason, the likely cause is because the model has searched for the solution with the smallest radius deviation, which happens to be one with period 2π. Maybe a configuration with the desired period of π is possible, except it has a greater radius variation than that which has

been output. To rectify this, the previously discussed way to improve the algorithm (give a period of π) could be used, whereby solutions are found where the radius/angular velocity is minimum at 0 and $\pm 2\pi$, and maximum at $\pm\frac{\pi}{2}$.

4.4.3 Near Stable - Results Section 3.2.3

The graphs show a clear resemblance to those provided in the main results section (two peaks over a 2π period such as in Figure 32 for example). However, they are imperfect in that the peaks are at different heights, and the plots do not reconnect with themselves when returning to the initial angle of $\theta = 0$, due to precession of the orbits. 100 iterations, four times more than the default 25, were used in the velocity corrector algorithm in an effort to gain stability, to no avail. This is likely because, once at 25 iterations the searching algorithm is already working in such a small range ($0.2^{25} = 3.36 \times 10^{-18}$) that any more iterations provides a negligible difference to the results ($0.2^{100} = 1.27 \times 10^{-70}$). It is worth to note that this irregularity was made to occur when the Outer Bar mass is increased in proportion relative to that of the Inner Bar. The system goes from stability, as seen in the early results, to slight instability as seen here. If the ratio is further increased the system becomes completely unstable and unrecognisable in comparison to the earlier (stable) results. This solidifies the notion that stability is obtained more easily in a gravitational system when the mass distribution **decreases** as radius increases.

4.5 Model with Realistic galaxy Parameters

The torque (Q) values within the referenced study [1] range from ≈ 0.1 to ≈ 0.5. Using the static model Q value derived in section 2.7, this translates to mass ratios (between the central and bar mass) which span from ≈ 10 to ≈ 2.5. What is useful about this result is that models which use these mass ratios have already been explored in the previous subsection 3.1. For example, the model which was used in the method section as a stable example (also used as the first data point in the 'Varying the Central Mass' section 3.1.1) involves a parameter configuration whereby the Central Mass = 20 and the Outer Bar Mass = 2. This gives a mass ratio of 10, which is equal to the upper bound of mass ratios in the referenced study. As another example, the third entry in the 'Varying the Central Mass' section 3.1.1 has a mass ratio between the Central mass and Outer Bar equal to 2.5, which is equal to the lower bound of the mass ratios found from the referenced study. The majority of the investigated models fall within these bounds.

With regards to the initial radii of the bars (the other parameter of the system) this space has been covered in the previous section 4.3 (from $r = 7$ to $r = 2.875$). Of course, since this model is dimensionless, these outer bar radii values also define the proportional size of the inner bar, since the two radii parameters are **relative** to each other. It is known that barred galaxies have relative bars sizes which fall within these bounds just referenced (r values in page 17 of [1]), meaning that the bar size parameter space has been fully covered.

The parameter space for observed double bar galaxies has been fully covered. This means that the models created in this project could potentially be used to determine the proportional changes in the radii and angular velocities of Bars in a realistic galaxy (if the torque value for a real galaxy was known).

5 Conclusion

In conclusion, I have successfully created a numerical simulation which models the radius and angular velocity oscillations of the Inner and Outer Bars of a double barred galaxy. Multiple physical assumptions were made (binary mass bars; end of bars mirror each other in movement; fixed mass at origin) in order to avoid the problem encountered with N-Body simulations whereby it is not possible to control the properties of the Inner Bar by adjusting the initial conditions. Real mass proportions for the system were found by calculating the torques produced by the bars in a theoretical model and comparing these to real observed values. It was inferred that if the theoretical and realistic system had the same torque, they had the same mass ratios.

It was determined that as the central mass is decreased, the oscillations for both bars grow due to their increased influence over each other. Additionally, it was found that the central mass could be decreased indefinitely and still result in a stable system, due to the constraint whereby it is set to be fixed to the origin. As the central mass was decreased to insignificant values with respect to that of the Inner and Outer Bars, their subsequent oscillations eventually ceased to change any further. This was because the majority of their felt force came from the other Bar (which was unchanging in this section since the masses were kept constant).

As the Inner Bar mass is decreased, the oscillations for the Inner Bar increase slowly. The reason for the increase is because the Outer Bar's mass grows in relative proportion as the Inner Bar's mass is decreased, and so has a greater oscillatory influence over it. This effect is slow however due to the close proximity of the Inner Bar to the Central Mass, which acts to reduce these oscillations. The oscillations for the Outer Bar decrease rapidly (still linear) in comparison as the Inner Bar mass is decreased, due to basic Newtonian gravity where the force decreases linearly. The oscillations for the Outer Bar approach 0, as the Inner Bar mass approaches 0, since the Outer Bar will therefore approximate to just itself and the Central Mass (perfectly circular orbits possible).

As the Outer Bar's initial radius is decreased, both bars see a rapid increase in oscillations which limit to infinity as the Bars become closer. This is related to the inverse square law ($\frac{1}{r^2}$), where the forced oscillations rapidly rise as r decreases to smaller values.

These findings are very appreciable because they would not have been made possible with use of an N-Body simulation, since the formation of Inner Bars within them are rather stochastic, therefore not allowing easy control of the parameters of the formed Bars. In this study however, found are clear values for the oscillations of the two bars as a function of certain parameters (central mass, inner bar mass, outer bar initial radius).

The limitations of this study partly reside within the assumptions made at the start. When approximating the bar as a binary (all of the mass is located at the ends) it of course misrepresents the mass distribution of the bar (even though it is a good approximation), since in reality there is matter located all along the bar's length. This assumption means that the influence from the bars will be particularly different at certain points. For example, when the Bars are perpendicular feel less of a mutual force than they should do (in reality), since the mass of the Bar is (unnaturally) located at the ends. In a realistic system the portions of the two bars which reside at low radii will still be relatively close to each other when aligned perpendicularly, which would give a greater force than which is found with the assumption used in this project. Essentially, approximating as a binary simplifies the oscillations of the bars with respect to each other, since if a bar with

an accurately distributed mass was modelled the gravitational system would naturally be more complex.

Fixing the central mass at the origin was also a clear limitation since it allowed the mass to be decreased indefinitely without the system suffering any stability problems. This is of course not representative of a realistic galaxy since the whole system would rapidly become unstable if the central mass was reduced significantly (Lack of heavy stabilising mass in the centre).

Another clear limitation is with the velocity correction algorithm and its mechanism of action (which has previously been discussed). If more specific constraints were placed on the algorithm, such as for it to search for solutions with radii minimums at 0 and $\pm 2\pi$, and maximums at $\pm\frac{\pi}{2}$ (sinusoidal), opposed to just reducing the overall radii variation, a greater range of more unstable parameters could potentially be investigated (in the sinusoidal oscillation form which is desired).

Future investigations of this type could use a different approach whereby the realistic masses and positions of the constituent objects in the system could be directly input into the model. This would give real values for the oscillations of the bars. Of course, these realistic masses and positions would have to be researched/derived.

Another avenue of further research could be to observationally search for barred galaxies across the universe and see if they adhere to the effects which we have seen. For example, a survey could be carried out for galaxies with similar bar length scales as those modelled in 3.1.3 (Varying the Outer Bar Initial Radius). In the model, it was found that smaller relative bar scales resulted in much greater bar oscillations than those seen for longer bar scales. The overall morphologies/kinematics of real galaxies which fall within the modelled bar length parameter space could be collectively compared. If there is **no significant trend** in morphology (based on the bar length), research could be carried out as to why this is the case, since galaxies across this parameter space would be projected to have different morphologies/kinematics (assuming that the bar oscillations affect the galaxy on an observable scale). If there **is** a trend in morphology based on relative bar length, it can of course be inferred that the reason that this happens is due to the effects that the different oscillations of the bar systems have upon their respective host galaxy.

References

[1] S. Díaz-García, H. Salo, E. Laurikainen, and M. Herrera-Endoqui. Characterization of galactic bars from 3.6 μm S^{4}G imaging. *AAP*, 587:A160, March 2016.

[2] Tod R. Lauer et al. New horizons observations of the cosmic optical background. *The Astrophysical Journal*, 906(2):77, jan 2021.

[3] Kartik Sheth et al. Evolution of the bar fraction in COSMOS: Quantifying the assembly of the hubble sequence. *The Astrophysical Journal*, 675(2):1141–1155, mar 2008.

[4] Paul B. Eskridge and Jay A. Frogel. What is the True Fraction of Barred Spiral Galaxies? *Astrophysics and Space Science*, 269:427–430, December 1999.

[5] Peter Erwin. Double-barred galaxies, 2009.

A Appendix - Presentation Questions

A.1 "How do the values that you chose for say m1 and m2 (mass of both bars?) correspond to real data?"

In order to make the masses of the Bars representative of those seen in a real system, a method was used whereby the Bar's torque value (Q) was calculated (section 2.7), with use of a static model which finds various force components of a test mass in a bar system. This torque value changes depending on the mass ratio between the central mass and the mass of the bar. Since the torque is a force ratio (therefore being dimensionless) it can be compared to torque values for real galaxy observations. S. Diaz Garcia et al. [1] provides numerous such torque values for observations of real barred spiral galaxies. Varying the mass ratios in the model to obtain a theoretical torque value which corresponds to a torque value found in the study, it can be inferred that the mass ratios found from the theoretical model and the real bar system are the same. This therefore allows the implementation of realistic mass **ratios** in the dynamic bar simulation.

A problem with this method is that the torque values given in the study are for those in a single (primary) bar system. This is because the secondary bar is too small to clearly observe (if the galaxy in question even has one). To get around this, the static model was implemented in two different instances. One was used to obtain the inner bar mass ratio (expressing the inner bar as an outer bar), the other was used to find the outer bar mass ratio (comparing theoretical torque values to realistic). If two separate ratios were found which go as $\frac{\text{Central Mass}}{\text{Inner Bar Mass}}$ and $\frac{\text{Central Mass}}{\text{Outer Bar Mass}}$ a full double bar model could be constructed (all of the masses are mathematically connected). An inherent flaw in this solution is that the masses of the two bars are determined separately in the static model (as a ratio to the central mass). In reality, the bars will be gravitationally influencing each other and so the torque values may different if this was taken into account.

Another potential flaw is that the theoretical torque values for the inner (secondary) bar are being compared to those which have been observed for a primary bar. This therefore assumes that the inner and outer bars behave equally relative to their torques. It is not fully known if this is the case (the inner bar may act differently since it is very close to the centre). Further research could be carried out which either confirms or denies if this assumption is allowed. If yes, the referenced study could be used to find the masses of the inner bar. If no, another avenue of mass determination would have to be conceived.

A.2 "How can you verify that the output of the odeint tracking software is representative of the behaviour of a physical system, and that the software is being used correctly?"

Physical systems must obey the law of the conservation of energy $E_k + E_p = \text{Constant}$. The extent at which the simulation conserves the total energy is investigated in section 2.3.1. It was found that whilst using the default 'odeint' parameters, the deviation of total energy over a longer time period than was used in the main results (at least 10x longer) was relatively small, at an accuracy level of 10^{-6}. The commonly accepted accuracy value is 10^{-8} however, and so the accuracy of the differential equation solver 'odeint' was increased by varying certain parameters such as the time step (decreased) and the error checking (increased). When these parameters were changed, an accuracy of 10^{-13} was attained, which is extremely accurate (well into the range commonly accepted).

Since this is a numerical method it is impossible to conserve energy completely due to the fact that a 'continuous'/infinitesimal time step is not possible, therefore meaning that small errors will be accumulated over time. These can be minimised however by doing certain things such as decreasing the time step as much as possible, which were successfully carried out.

Although it wasn't performed in this project, another possible verification is through checking if the angular momentum is conserved. Just like the total energy, this must be conserved also. This is calculated via $L = mvr$. This value could be added up for every constituent, at every moment in time and checked to see if it stays the same over time. Of course, since this is a numerical simulation it is bound to change slightly, but as long as it only deviates by small values (like those just referenced) it can be inferred that the system is working well.

B Appendix - Project Proposal/Plan

Student Name: George Scannell – 201458660

Project Title: Double Binary as a Model of a Double Bar

Supervisor: Witold Maciejewski

Axially symmetric disks (containing stars and gas) are generally unstable in nature, due to the Toomre parameter which governs the dynamic stability of a system and resistance to collapse (with regards to gravity, thermal pressure, shear force etc). In many cases the Toomre parameter of galactic disks of these nature falls under a certain threshold, and collapse into a central bar occurs (these are more stable structures). With regards to this bar, assuming that stars do not collide, but gas does (total volume much greater for gas), it can be assumed that the torque of the bar will take the outer gas off of their circular orbits, causing collisions and a subsequent loss of angular momentum, which will eventually result in the reduction of orbital radii for the gas, and collapse into a second axially symmetric disk at the centre of the bar. The previously mentioned logic referring to the instability of disks of these nature can be applied again, resulting in the collapse of this disk into a secondary bar.

This project "Double binary as a model of a double bar" aims to measure and quantify any variations in rotational velocities and/or deformations (over time) of a central double bar of a spiral galaxy. For simplification, each bar will be assumed to consist of a dipole mass system, where half of the mass of the bar is at one end, half at the other. This works well as a simplification since much of the influence of the bar arises from each end due to the higher angular momenta. The rest of the mass of the galaxy can also be assumed to be located in a condensed, centralised location within the centre of the structure. Simulations such as these, albeit simplified, can be applied to real, observed galaxies and be used to predict phenomena and therefore solidify understanding. Additionally, this simplification holds weight due to the fact that a direct (full) n-body simulation of a realistic number of stars and/or gas particles is not possible due to current computing power restraints. Therefore, the resolution will need to suffer at the cost of completing the simulation in finite time. Of course, this model will only provide a rough parameter range for possible double bars.

Below is a table outlining the general timeline for this project, showing when parts should be started and completed. This is a general tool to assist with time management, with it being highly likely that there will be deviations from this plan i.e. starting some parts early/late or doing two tasks simultaneously. Organising into weeks greatly simplifies the matter. This table is also represented in gantt form via the tabs at the top of this channel. (Open with desktop – to increase date use scroll bar near the top)
A risk assessment is also provided as a word document.

Week/Date	Task	Description
1, 2	Background Reading and Project Outline creation (POA)	Reading on project at hand, and time period for project description and timetable creation (proposal)
11/02/22	Project Proposal and Risk Assessment due date	
2, 3	Formulating the problem	Accumulating a set of equations to describe the system (pen and paper), as well as the initial conditions – in preparation for the programming

3, 4	Coding In Equations	Putting the equations derived during the previous weeks into a program, ready to be run. Timeline for the following weeks are only a guideline, since tests for example will need to be performed whilst the equations are being coded in.
5	Fine Tuning and Test Runs	Testing code and altering initial parameters to determine optimal values
6, 7	Production Runs	Production of data using predetermined parameters
8, 9	Analysis of Results	Analysis of produced data, implications etc.
8, 9	Presentation Preparation	Slides, notes, script etc.
23/03/2022	Presentation	Presentation on the project so far
10, 11, 12	Report Writing	Report writing (Overleaf – latex) and final touches. Project portfolio and report due on this date.
13/05/2022	Final Report Due Date	

C Appendix - Full Code

Links to the entire python code used in this project (different formats/locations of storage):

(Liverpool Uni Teams Server) - Source code in .ipynb format: https://theuniversityofliverpool.sharepoint.com/:u:/s/PHYS379-202122-II-O365-Team-Scannell/EYj7m_frBfNCmVoxu9fLNOIBmyT3jlSAmY7rYNNQWhNRYw?e=dB7FN4

(Liverpool Uni Teams Server) - code in.html format: https://theuniversityofliverpool.sharepoint.com/:u:/s/PHYS379-202122-II-O365-Team-Scannell/EbzXngC9ifVLmykivuD34kkByNrYjK7nQ6vrd2RBJG2ATQ?e=SUyLCh

(Liverpool Uni Teams Server) - code in .pdf format: https://theuniversityofliverpool.sharepoint.com/:b:/s/PHYS379-202122-II-O365-Team-Scannell/EQ5328OY431OnFj_q4LycyQB2CvmHO7fKHPXV1OH2z9GdA?e=CVTRqu

GitHub repository containing code in ipynb. and pdf. formats: https://github.com/scivern/BSc-Project.git

D Appendix - Risk Assessment

UNIVERSITY OF LIVERPOOL

RISK ASSESSMENT FORM

School/Department: Physics	**Building:**
Task: 3rd Year Astro Project	
Persons who can be adversely affected by the activity: Student and Supervisor	

Section 1: Is there potential for one or more of the issues below to lead to injury/ill health (tick relevant boxes)

People and animals/Behaviour hazards

Allergies		Too few people		Horseplay		Repetitive action	/	Farm animals	
Disabilities		Too many people		Violence/aggression		Standing for long periods		Small animals	
Poor training		Non-employees		Stress		Fatigue	/	Physical size, strength, shape	
Poor supervision		Illness/disease		Pregnancy/expectant mothers		Awkward body postures	/	Potential for human error	
Lack of experience		Lack of insurance		Static body postures	/	Lack of or poor communication		Taking short cuts	
Children		Rushing		Lack of mental ability		Language difficulties		Vulnerable adult group	

What controls measures are in place or need to be introduced to address the issues identified?

Identified hazards	**What controls are currently planned or in place to ensure that the hazard identified does not lead to injury or ill-health?**	**RISK SCORE**			**Is there anything more that you can do to reduce the risk score in addition to what is already planned or in place?**	**RESIDUAL RISK SCORE**		
		L	**C**	**R**		**L**	**C**	**R**
Pain from sitting still too long on computer (posture)	None	2	2	4	Take breaks, move around periodically	1	2	2

Repetitive strain (mouse/keyboard)	None	1	2	2	Take breaks, use less risky interfaces i.e specialist mice	0	2	0

L = likelihood; C = consequence; R = overall risk rating

Section 2: Common Workplace hazards. Is there potential for one or more of the issues below to lead to injury/ill health (tick relevant boxes)

Fall from height		Poor lighting		Portable tools		Fire hazards		Chemicals		Asbestos	
Falling objects		Poor heating or ventilation		Powered/moving machinery		Vehicles		Biological agents		Explosives	
Slips, trips, falls		Poor space design		Lifting equipment		Radiation sources		Waste materials		Genetic modification work	
Manual handling		Poor welfare facilities		Pressure vessels		Lasers		Nanotechnology		Magnetic devices	
Display screen equipment	/	Electrical equipment	/	Noise or vibration		Confined spaces		Gases		Extraction systems	

Temperature extremes		Sharps		Drones		Cryogenics		Legionella		Robotics	
Home working	/	Poor signage		Overseas work		Overnight experiments		Unusual events		Community visits	
Late/lone working		Lack of/poor selection of PPE		Night work		Long hours	/	Weather extremes		Diving	

What controls measures are in place or need to be introduced to address the issues identified?

Identified hazards	What controls are currently planned or in place to ensure that the hazard identified does not lead to injury or ill-health?	RISK SCORE			Is there anything more that you can do to reduce the risk score in addition to what is already planned or in place?	RESIDUAL RISK SCORE		
		L	C	R		L	C	R
Eye pain from looking at screen	None	1	1	1	Take breaks	0	0	0

Electrical overload	Not stacking extension cables into each other	1	2	**2**	Unplug appliances not in use	1	1	1
Working too long can cause fatigue/tiredness – in kitchen dangers may occur	None	1	2	2	Not working too long/having breaks	1	1	1

L = likelihood; C = consequence; R = overall risk rating

Section 3: Additional hazards: are there further hazards NOT IDENTIFIED ABOVE that need to be considered and what controls are in place or needed? (list below)

Identified hazards	What controls are currently planned or in place to ensure that the hazard identified does not lead to injury or ill-health?	RISK SCORE			Is there anything more that you can do to reduce the risk score in addition to what is already planned or in place?	RESIDUAL RISK SCORE		
		L	C	R		L	C	R

Section 4: Emergency arrangements (List any additional controls that are required to deal with the potential emergency situation)

Emergency situation	Additional control required

Risk assessor (signature).....Date..... Authorised by (signature).....Date.....

COMPLETING THE RISK ASSESSMENT FORM

- School/Department – note down the School and/or Department where the task is being carried out
- Building – note the specific building(s) where the task is being carried out
- Task – specific clearly the task being carried out
- People would could be adversely affected – think of all the people who could be affected by what you are doing
- Hazards – tick all the relevant hazards in sections 1 and 2. If ticked you will need to log what controls are already in place to protect people from the hazard and what extra controls are required (if any) in the relevant control boxes. As part of the control measures you will need to make a decision of the level of risk based on the tables below. NB – it is likely that other hazards may exist that are not captured in sections 1 and 2. Section 3 should be used to capture any additional hazards and controls not listed in Sections 1 and 2.
- Emergency procedures – list the basic procedures that need to be taken if a critical incident occurs
- Signature – the people completing and approving the assessment must sign the relevant boxes at the end of the document

Likelihood	
1	Very unlikely
2	Unlikely
3	Fairly likely
4	Likely
5	Very likely

Consequence	
1	Insignificant – no injury
2	Minor – minor injuries needing first aid
3	Moderate – up to seven days absence
4	Major – more than seven days absence; major injury
5	Catastrophic – death; multiple serious injury

Consequences						
	5	5	10	15	20	25
	4	4	8	12	16	20
	3	3	6	9	12	15
	2	2	4	6	8	10
	1	1	2	3	4	5
		1	**2**	**3**	**4**	**5**
		Likelihood				

- Additional control required - list any additional control required that will reduce the risk rating score. Ensure responsibilities for tasks and timescales are added
- Residual risk score – re-calculate the risk score after the introduction of the additional controls. Compare residual risk score with table below. Take further action if necessary.

ACTION TO BE TAKEN	
1-4 Acceptable	No further action but ensure controls are maintained
5-9 Adequate	Look to improve at next review.
10-16 Tolerable	Look to improve within specified timescale
17-25 Unacceptable	Stop activity and make immediate improvements